Cell

Top-Down Control of Sweet and Bitter Taste in the Mammalian Brain

Graphical Abstract

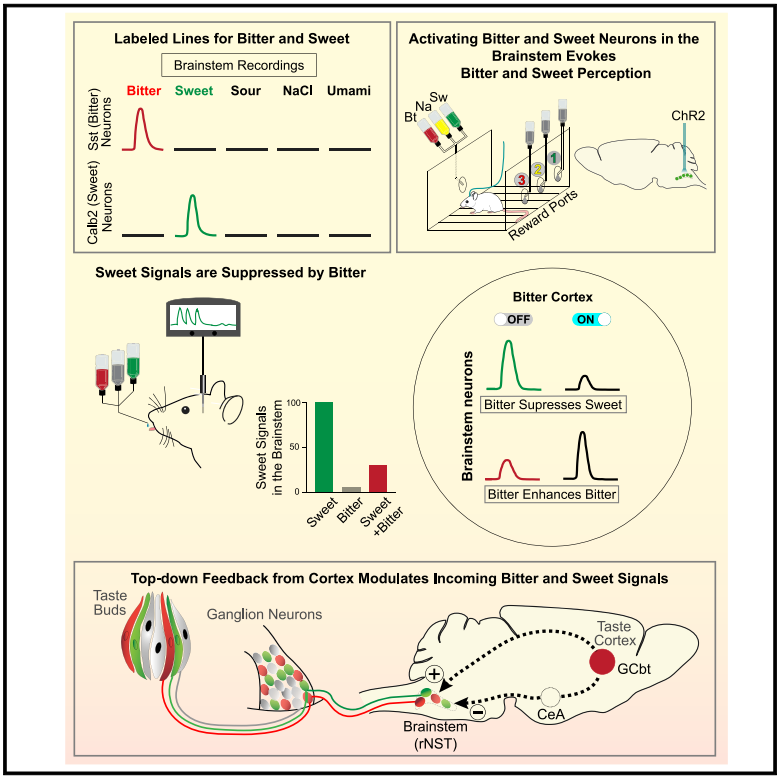

Highlights

- Sweet and bitter are represented in the brainstem by genetically distinct neurons
- SST^{+} and CALB2^{+} neurons in the brainstem carry bitter and sweet signals to the cortex
- Feedback from bitter cortex amplifies bitter but suppresses incoming sweet taste signals
- Cortical feedback via amygdala ensures bitter-evoked behavioral aversion remains robust

Authors

Hao Jin, Z. Hershel Fishman, Mingyu Ye, Li Wang, Charles S. Zuker

Correspondence

cz2195@columbia.edu

In Brief

Labeled line circuits transmitting sweet and bitter signals from the tongue to the cortex are modulated by top-down feedback. Bitter taste triggers cortically evoked suppression of sweet inputs but enhances bitter signals in the brainstem to control taste behaviors.

Jin et al., 2021, Cell *184*, 257–271
January 7, 2021
https://doi.org/10.1016/j.cell.2020.12.014

CellPress

Cell

CellPress

Article

Top-Down Control of Sweet and Bitter Taste in the Mammalian Brain

Hao Jin,[1] Z. Hershel Fishman,[1,2] Mingyu Ye,[1,2] Li Wang,[1] and Charles S. Zuker[1,3,*]

[1]Howard Hughes Medical Institute, Department of Biochemistry and Molecular Biophysics and Department of Neuroscience, Columbia College of Physicians and Surgeons, Columbia University, New York, NY 10032, USA

[2]These authors contributed equally

[3]Lead Contact

*Correspondence: cz2195@columbia.edu

https://doi.org/10.1016/j.cell.2020.12.014

SUMMARY

Hardwired circuits encoding innate responses have emerged as an essential feature of the mammalian brain. Sweet and bitter evoke opposing predetermined behaviors. Sweet drives appetitive responses and consumption of energy-rich food sources, whereas bitter prevents ingestion of toxic chemicals. Here we identified and characterized the neurons in the brainstem that transmit sweet and bitter signals from the tongue to the cortex. Next we examined how the brain modulates this hardwired circuit to control taste behaviors. We dissect the basis for bitter-evoked suppression of sweet taste and show that the taste cortex and amygdala exert strong positive and negative feedback onto incoming bitter and sweet signals in the brainstem. Finally we demonstrate that blocking the feedback markedly alters responses to ethologically relevant taste stimuli. These results illustrate how hardwired circuits can be finely regulated by top-down control and reveal the neural basis of an indispensable behavioral response for all animals.

INTRODUCTION

Hardwired neural circuits participate in a broad range of behaviors, including responses to external chemosensory cues (Root et al., 2014; Yarmolinsky et al., 2009) and to internal signals (Anderson, 2016; Zimmerman et al., 2017). The mammalian taste system is a prominent example of a major sensory system hardwired to trigger predetermined actions and behaviors, such as our innate attraction and consumption of sweet compounds and aversion to bitters (Scott, 2005; Yarmolinsky et al., 2009).

Sweet and bitter chemicals are first recognized by dedicated taste receptor cells (TRCs) on the tongue and palate epithelium. The activated TRCs then transfer their signals through 4 additional neuronal stations to ultimately reach the taste cortex (Spector and Travers, 2005; Yarmolinsky et al., 2009); first from TRCs to matching ganglion neurons (i.e., sweet TRCs to sweet neurons and bitter TRCs to bitter neurons). These signals then enter the brain by synapsing with targets in the rostral nucleus of the solitary tract (rNST) of the brainstem. Thereafter, information travels to the parabrachial nucleus (PBN), the thalamus, and finally the taste cortex, where sweet and bitter tastes are represented by separate populations of cortical neurons (Chen et al., 2011).

A fundamental question about innate behaviors is how they are regulated. The demonstration that a neural circuit operates via labeled lines wired to trigger stereotypic, innate behaviors does not imply that it is not subjected to modulation or plasticity; it means that these circuits evoke predetermined responses requiring no prior learning or experience (Scott, 2005; Yarmolinsky et al., 2009). Here we show how circuits guiding responses to the two most salient taste qualities, bitter and sweet, are critically modulated by top-down control.

RESULTS

The Taste Cortex and Amygdala Send Prominent Projections to the Brainstem

It is well recognized that the evolution of bitter taste receptors reflected the need to detect and prevent ingestion of harmful chemicals (Antinucci and Risso, 2017; Dong et al., 2009; Nei et al., 2008). But how does the brain ensure behavioral rejection of a bitter tastant in the presence of an appealing sweet stimulus (Figures 1A and S1A)? At the level of peripheral taste circuits (i.e., TRCs and ganglion neurons), the neural responses to mixtures of sweet and bitter exhibit no significant cross-modulation (Barretto et al., 2015). Therefore, to uncover targets for potential bitter-evoked modulation of sweet taste in the brain, we labeled neurons in the bitter cortical field (an area of the taste cortex preferentially responsive to bitter stimuli, hereafter referred to as GCbt) (Chen et al., 2011; Peng et al., 2015) and in the central amygdala (CeA) with different fluorescent tracers and examined their projections by whole-brain clearing and rapid 3D imaging with light-sheet fluorescent microscopy using clear, unobstructed brain imaging and computational analysis (CUBIC) (Susaki et al., 2014; Wang et al., 2018). We chose these two brain areas because the taste cortex and the amygdala are key neural

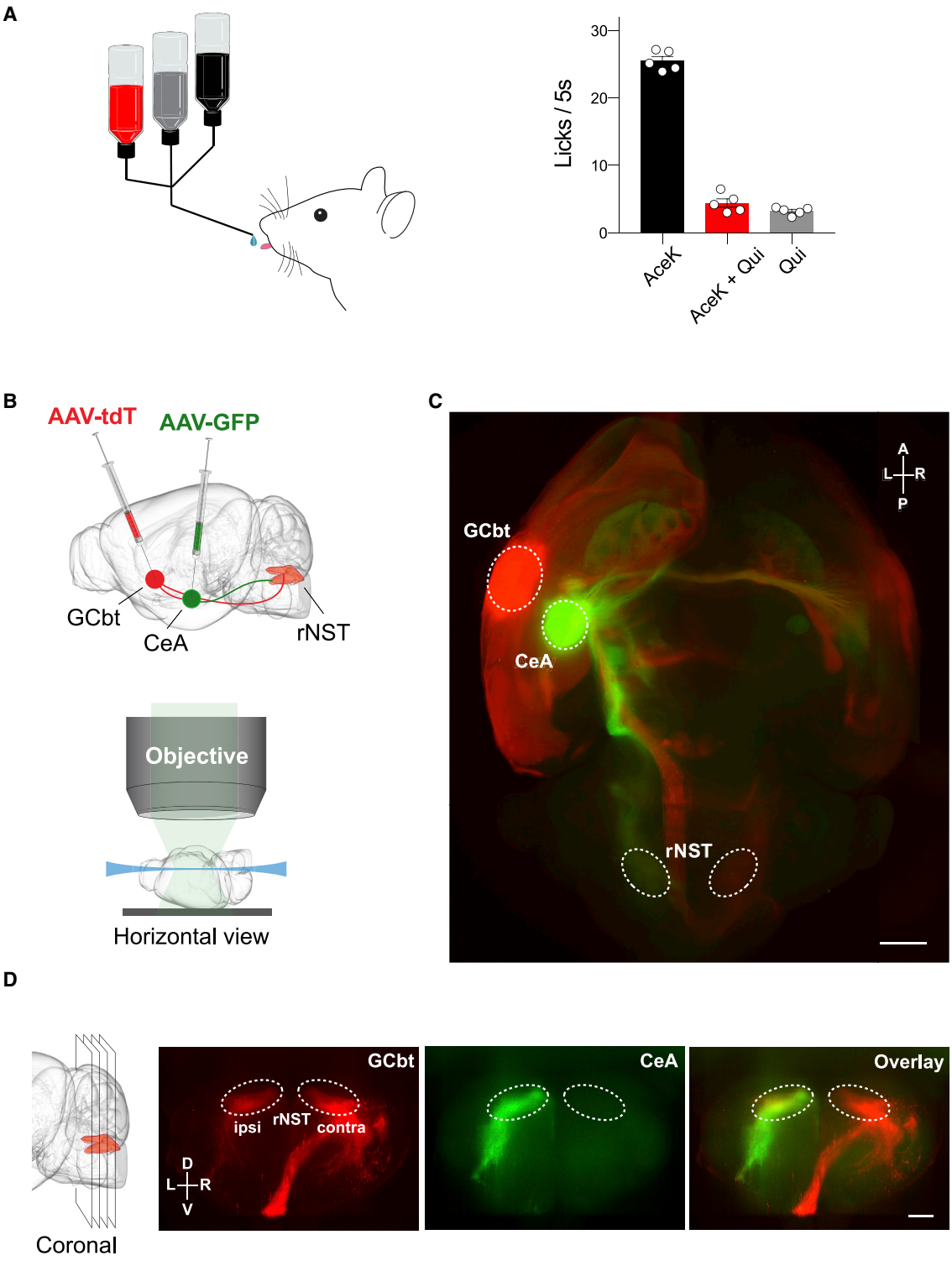

Figure 1. Top-Down Projections from the Bitter Cortical Field and CeA to the rNST

(A) Bitter suppresses behavioral attraction to sweet tastants. Prior to testing, animals were motivated by food and water restriction (see STAR Methods for details). Animals were then exposed to licking sessions consisting of random trials of sweet, bitter, or a mix of the two tastants. The graph shows quantification of the lick responses to the sweet stimulus alone (4 mM AceK [acesulfame potassium]), bitter alone (5 mM Qui [quinine]), and the sweet plus bitter mix (4 mM AceK plus 5 mM Qui). n = 5 mice; values are means ± SEM, one-way ANOVA followed by Tukey post hoc test, $p < 0.0001$ (sweet versus bitter and sweet versus mix), $p > 0.2$ (mix versus bitter). See also Figure S1A.

(legend continued on next page)

substrates encoding the identity and the valence of a taste stimulus (i.e., "what is it?" and "is it good or bad?") (Wang et al., 2018; Bales et al., 2015; Blonde et al., 2015).

Our results (Figures 1B–1D and S1B–S1N) showed that the GCbt and CeA exhibit prominent projections all the way down to the rNST in the brainstem, the first site of entry of sweet and bitter taste signals from the periphery into the brain (Spector and Travers, 2005; Hayama and Ogawa, 2001; Whitehead et al., 2000). These long-range projections to the brainstem immediately suggested a strategy for top-down control of taste behaviors.

Sweet and Bitter Neurons in the rNST

To identify the neurons representing sweet and bitter taste in the rNST, we infected rNST neurons with an AAV harboring a Synapsin1::GCaMP6s construct to drive expression of the activity reporter in most neurons of the rNST (Chen et al., 2013; McLean et al., 2014; Schoch et al., 1996) and recorded responses to various taste stimuli using fiber photometry (Gunaydin et al., 2014; Figure 2A). To ensure that all taste stimuli were effectively delivered to the tongue, we used an intra-oral cannula stimulus delivery system (Phillips and Norgren, 1970). As anticipated, the rNST houses neurons exhibiting robust responses to all five basic taste qualities (Figures 2B and S2A). Next we searched the publicly available Allen Mouse Brain Atlas (https://www.alleninstitute.org/) for genes that mark subsets of rNST neurons (Zhang et al., 2019). We then infected the rNST of candidate Cre driver lines with an AAV carrying a Cre-dependent GCaMP6s activity reporter (Chen et al., 2013) and showed that somatostatin-positive neurons (*Sst*) (Taniguchi et al., 2011; Thek et al., 2019) are tuned to bitter tastes, whereas Calbindin 2-positive neurons (*Calb2*) (Taniguchi et al., 2011) respond selectively to sweet tastants (Figures 2C and 2D). Importantly, the neurons expressing *Sst* in the rNST are different from those expressing *Calb2*, with no overlap (Figure S4). Moreover, these two populations of neurons are intermingled, with no discernable topographic organization. Of course, labeled line coding is independent of topography. Hence, neurons representing the different tastes can exhibit significant topographic segregation (like sweet and bitter in the taste cortex) (Chen et al., 2011) or be intermingled like in the rNST without affecting their labeled line tuning properties.

Genetically Defined Neurons for Sweet and Bitter Taste in the Brainstem

To demonstrate that the taste responses of *Sst*- and *Calb2*-expressing neurons originate from selective activation of bitter and sweet TRCs on the tongue, we repeated the fiber photometry recording experiments in animals lacking the taste signaling channel TRPM5; this ion channel is required for bitter and sweet but not sour or salty taste (Damak et al., 2006; Zhang et al., 2003). Indeed, all bitter responses from *Sst*-expressing neurons and all sweet responses from *Calb2* neurons were abolished in the *Trpm5* knockout animals (Figures S2D–S2F).

If the *Sst* and *Calb2* populations in the rNST are the conduits of bitter and sweet taste from the periphery into the brain, then their selective ablation should abolish behavioral responses to bitter and sweet stimuli, respectively. Thus, we engineered mice where these brainstem neurons were genetically removed by targeting a Cre-dependent diphtheria toxin A (DTA) virus to the rNST (AAV-Flex-DTA) (Wu et al., 2014) and tested the animals' responses to sweet and bitter stimuli before and after genetic ablation (see STAR Methods for details).

Freely moving animals were trained to drink from a center spout delivering random presentations of water, bitter, sweet, or sour stimuli (Zhang et al., 2003; Figure 3A); to motivate sampling of aversive stimuli, animals were water deprived prior to the test (STAR Methods). As expected, control animals displayed aversion to bitter and sour compounds and attraction to sweet (Figures 3B, 3D, and 3E). However, after DTA-mediated cell ablation of *Sst* neurons in the rNST, the animals no longer avoided bitter and avidly drank bitter solutions, even at exceedingly high concentrations (5 mM quinine [Qui]) (Mueller et al., 2005; Figures 3C and 3D). In contrast, responses to other tastants, including aversion to sour and attraction to sweet, remained largely unaffected (Figures 3C and 3E). These data substantiate the *Sst* population as specifically required for mediating bitter taste responses. Next we engineered animals with ablated *Calb2*-expressing neurons in the rNST. These animals exhibited dramatic loss of attractive responses to sweet stimuli, as seen by using an immediate lick behavioral test (Figure 3F) or a two-bottle preference assay (Figure 3H), even when using exceptionally high concentrations of sweet tastants (e.g., 20 mM acesulfame potassium [AceK]) (Zhao et al., 2003). In contrast, the attractive responses to a different appetitive stimulus (low salt) and the aversive responses to bitter and sour stimuli were unimpaired (Figure 3G). These results validate the *Calb2* population as indispensable for behavioral attraction to sweet taste.

Sst and *Calb2* Neurons Represent Sweet and Bitter Taste in the Brainstem

If *Sst* and *Calb2* neurons are the neural substrates for the tastes of bitter and sweet in the brainstem, then their selective activation should drive the corresponding taste behaviors in the absence of any taste stimuli. Furthermore, in a taste discrimination assay, their selective activation should be recognized as a "bitter" or a "sweet" stimulus even when the animals are sampling only water.

We introduced channelrhodopsin-2 (ChR2) (Boyden et al., 2005) into the rNST of *Sst-cre* or *Calb2-cre* animals by targeted infection with an AAV-Flex-ChR2 virus and used a behavioral test

(B) To trace projections from the bitter cortical field (referred to as GCbt) and the amygdala (CeA [central amygdala]), anterograde viral tracers were injected into the GCbt (AAV-tdTomato) and CeA (AAV-EGFP), and their projections were analyzed by clearing followed by whole-brain imaging with light-sheet fluorescence microscopy; n = 3 animals. See Figures S1B–S1N for additional images.

(C) Maximum-intensity z stack of projections from the GCbt (red) and CeA (green) to the rNST in the brainstem (dotted areas). Scale bar, 1 mm.

(D) Expanded view of stacked coronal sections. The GCbt predominantly projects to the contralateral (contra) rNST (left panel, red), whereas the CeA projects to ipsilateral (ipsi) rNST (center panel, green); GCbt and CeA projections reach the rNST ventrally. The right panel shows the overlay; scale bar, 0.5 mm.

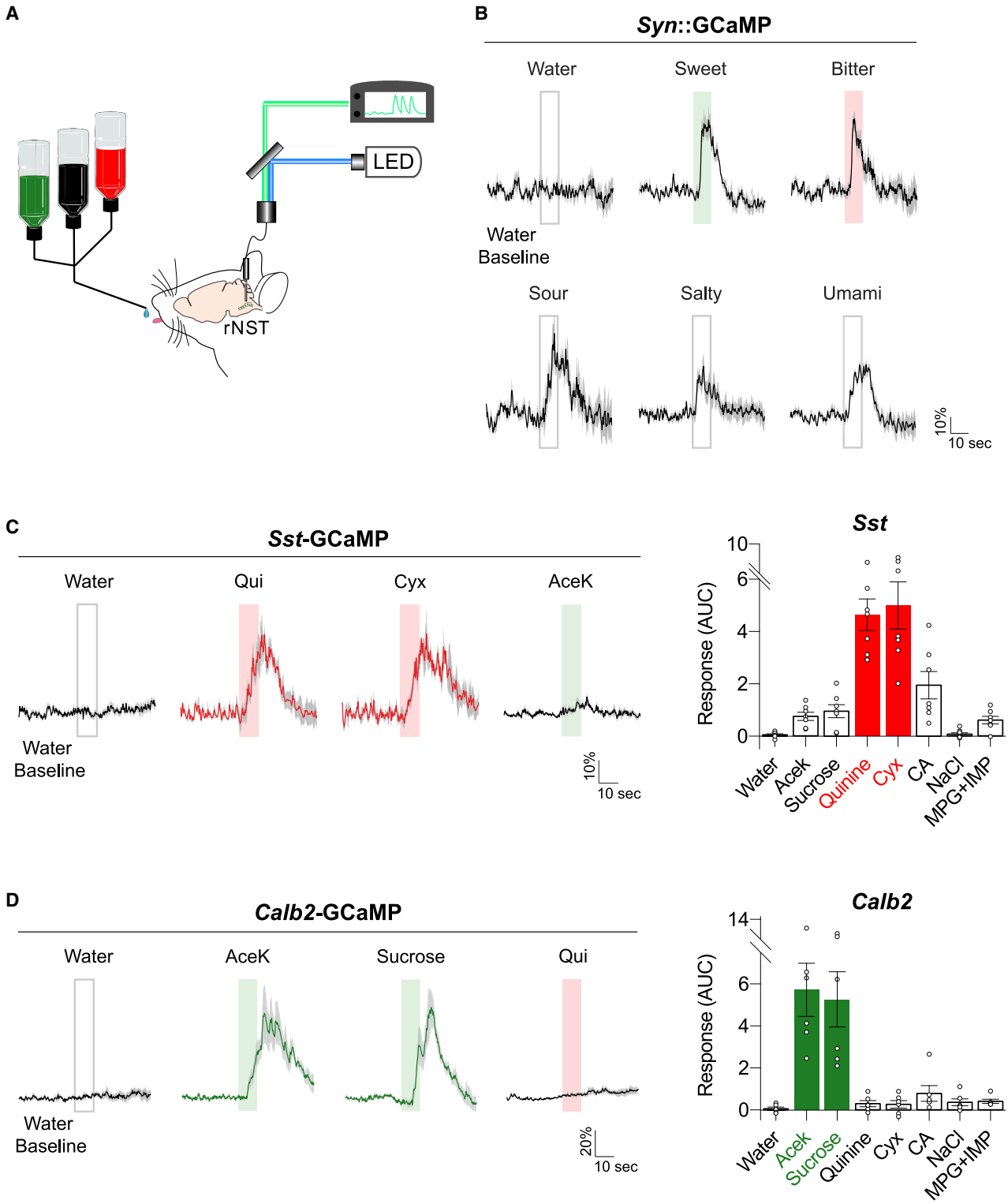

Figure 2. Characterization of Taste Neurons in the rNST

(A) Schematic of fiber photometry recordings of taste-evoked activity in the rNST. A synapsin (syn)-driven GCaMP6s reporter (AAV-Syn-GCaMP6s) was virally targeted to rNST neurons, and head-attached, awake animals were stimulated intra-orally with different tastants (STAR Methods; Figures S2A and S3A).

(legend continued on next page)

where ChR2-expressing animals were assayed for water drinking in a head-attached behavioral assay (Peng et al., 2015; see STAR Methods for details). Mice were subjected to testing sessions consisting of interleaved water-alone trials and water trials linked to lick-triggered photo-stimulation (Figure 4A). Notably, the laser shutter was placed under contact-licking operation; hence, the animal has control of its own stimulation during the light-on trials, and only self-stimulation would continue to trigger appetitive responses. In contrast, an animal would immediately terminate licking when contact-licking elicited aversion. Indeed, our results showed that optogenetic activation of *Sst* neurons triggered immediate suppression of licking (Figures 4B and 4C), whereas photo-activation of *Calb2* neurons elicited avid enhancement of licking (Figures 4D and 4E).

Next we trained animals to report the identity of a tastant by using a three-port behavioral assay (Wang et al., 2018). In this test, mice learned to sample a taste cue from a center spout (for example, random presentations of a sweet or a bitter chemical) and then report its identity by going to the right or left port; a correct response was rewarded with water (Figure 4F). This learned behavior requires that the animal samples the cue, identifies the tastant, and executes the appropriate choice in each trial. If activation of the *Calb2* and *Sst* neurons evokes internal representations resembling those to the orally applied sweet and bitter chemicals, then optogenetic stimulation should generalize to the learned response associated with that taste (Peng et al., 2015; Wang et al., 2018).

Animals expressing ChR2 in *Calb2* neurons were trained to recognize three taste cues: sweet (in this example, go left), bitter (go right), and water containing a very small amount of NaCl (we used 3 mM NaCl to differentiate it from the water reward, also go right). After training, mice successfully reported the identity of the testing solutions with over 90% accuracy (Figure 4G, see legend for details). Then we examined whether direct optogenetic activation of the *Calb2* neurons is also recognized as sweet. Our results (Figure 4G) demonstrated that animals reliably reported stimulation of *Calb2*-expressing neurons in the rNST as a sweet stimulus.

We performed similar experiments by optogenetically stimulating the *Sst* bitter neurons. In this case, animals were trained to recognize bitter (for example, go right), sweet (go left), and 3 mM NaCl (go left). Our results (Figure 4H) showed that optogenetic stimulation of *Sst*-expressing neurons in the rNST is consistently recognized as a bitter stimulus.

To further validate the capacity of the animals to correctly report the identity of the different tastants (and recognition of optogenetic activation of *Sst* neurons as a "bitter" stimulus), we also developed a four-port behavioral test consisting of a tastant delivery port and 3 separate response/reward ports, one for each tastant (Figure 4I). In this assay, mice were given random presentations of sweet, bitter, and salty stimuli, and they had to report the identity of the test stimulus in each trial by choosing the proper response port for each tastant (e.g., sweet = go to port 1, salt = go to port 2, bitter = go to port 3). After training (see STAR Methods for details), mice learned to successfully report the identity of each of the 3 tastants with over 80% accuracy; in contrast, a novel stimulus produced only random responses (Figure 4J). As anticipated, optogenetic stimulation of *Sst*-expressing neurons in the rNST was indeed recognized as a bitter stimulus (Figure 4J, light).

Top-Down Modulation of Sweet and Bitter Circuits

The functional validation of *Sst* and *Calb2* neurons in the rNST as essential conduits of bitter and sweet taste provided a substrate to dissect why and how bitter overrides a sweet stimulus in eliciting behavioral responses. The strategy was to introduce the GCaMP activity reporter in *Calb2* neurons in the rNST and determine how their response to a sweet tastant is altered when the animal is co-stimulated with a bitter tastant in a sweet-bitter mixed stimulus. The recordings shown in Figure 5A demonstrate that sweet taste responses from *Calb2* neurons are dramatically suppressed when a sweet stimulus is presented in the presence of a bitter tastant. In contrast, sweet stimuli have no effect on the activity of bitter rNST neurons (Figure 5B).

We hypothesized that the bitter-evoked suppression of incoming sweet taste signals in the rNST may be mediated by top-down modulation from the cortex to the rNST (Figures 1C and 1D) and, accordingly, predicted that optogenetic activation of the GCbt while the animal is sampling a sweet-only stimulus should result in suppression of the sweet-evoked signals in the rNST. Optogenetic activation of GCbt has been shown previously to reliably trigger bitter taste responses (including the appropriate orofacial actions, recognition of the optogenetic signal as a "bitter taste" in behavioral discrimination assays, lick suppression, and corresponding behavioral aversion) (Peng et al., 2015; Wang et al., 2018). Thus, we expressed ChR2 in excitatory neurons in the GCbt by using AAV- Ca^{2+}/calmodulin-dependent protein kinase II (CaMKII)-ChR2 (Peng et. al., 2015) and examined how their optogenetic activation modulates the tastant-evoked responses of sweet *Calb2* neurons. As predicted, our results demonstrated that stimulation

(B) Shown are sample average responses (black traces) ± SEM (gray) to water (baseline), 20 mM AceK (sweet), 5 mM Qui (bitter), 50 mM CA (citric acid, sour), 60 mM NaCl (salty), and 50 mM MPG (monopotassium glutamate) plus 1 mM IMP (inosine 5′-monophosphate) (umami); n = 4 animals (Figure S2A). Water is continuously flowing prior to and after tastant delivery.

(C) *Sst* neurons respond to bitter stimuli. Shown is tastant-evoked activity in animals expressing the GCaMP reporter (AAV-Flex-GCaMP6s) in *Sst-cre* neurons in the rNST (see also Figure S3A). Right panel: quantification of responses; water = baseline. AUC, area under the curve; n = 7 animals. Values are means ± SEM. The small responses to sweet likely represent activity evoked by avid licking to the sweet stimulus (in the cannula-based stimulation paradigm) because they are also present in water-deprived animals in response to water trials and even to dry-lick trials (Figure S2B); the small responses to acid stimuli (sour) are due to activation of bitter T2Rs by acid (i.e., the responses are eliminated by abolishing bitter signaling; Figure S2D) (Barretto et al., 2015; Zhang et al., 2019).

(D) *Calb2* neurons respond to sweet stimuli. Shown is tastant-evoked activity in animals expressing the GCaMP reporter (AAV-Flex-GCaMP6s) in *Calb2-cre* neurons in the rNST (see also Figure S3A). Right panel: quantification of evoked responses; water = baseline. n = 6 animals; Values are means ± SEM. See also Figure S2C.

Tastants used for (C) and (D): sweet, 20 mM AceK, 600 mM sucrose; bitter, 5 mM Qui, 0.2 mM Cyx (cycloheximide); sour, 60 mM CA; salty, 60 mM NaCl; umami, 50 mM MPG + 1 mM IMP. Shaded and open bars indicate the duration of taste stimuli (10 s). Scale, ΔF/F.

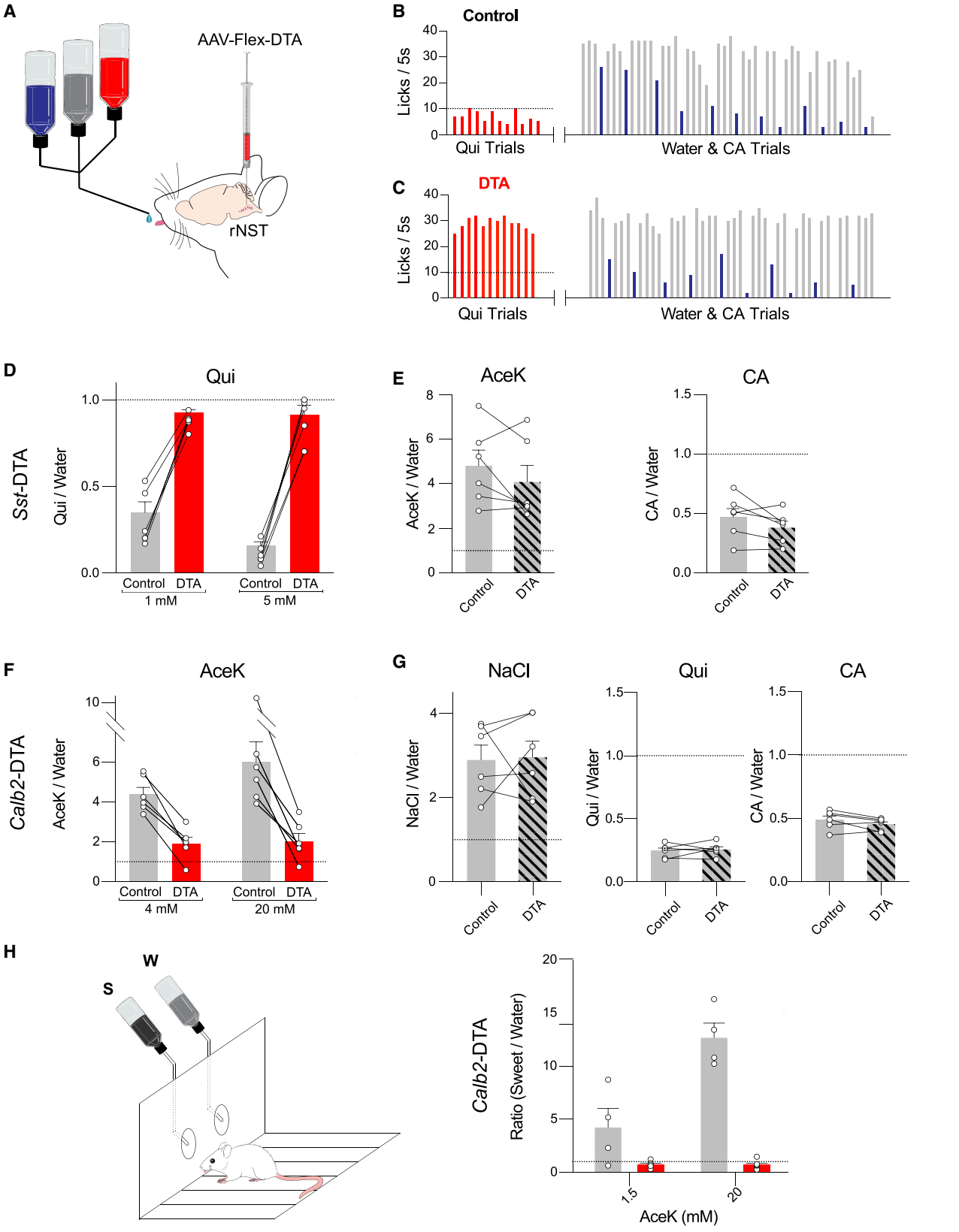

(legend on next page)

of the GCbt strongly suppressed propagation of sweet signals by inhibiting the activity of the sweet neurons in the rNST (Figure 5C). Notably, we also examined the effect of GCbt on bitter neurons in the rNST and uncovered a second feedback circuit: stimulation of GCbt significantly enhanced the activity of bitter-evoked activity in bitter-coding *Sst* neurons (Figure 5D). Thus, bitter signals, when they reach the taste cortex, feed back positively onto bitter neurons in the brainstem, amplifying the responses elicited by bitter tastants, while exerting negative feedback onto sweet-responding neurons, suppressing and minimizing sweet-evoked activity.

Inhibitory and Excitatory Feedback into Sweet and Bitter Brainstem Neurons

To uncover the physiological basis for the top-down feedback control from the cortex, we carried out patch-clamp recordings from individual bitter and sweet neurons in the rNST. We engineered mice where a tdTomato fluorescent reporter was targeted to *Sst* or *Calb2* neurons and recorded from the tdTomato-labeled cells in the rNST using a brainstem slice preparation (Hardaway et al., 2019; Petreanu et al., 2007; Figure 6A; see STAR Methods for details). Importantly, the same animals also expressed a ChR2-yellow fluorescent protein (YFP) construct in the GCbt (and, therefore, their projections to the brainstem expressed ChR2 and were marked by YFP expression). Our results demonstrated that *Sst* bitter neurons in the rNST indeed receive excitatory input from the GCbt (Figures 6B–6D and S6A–S6K). We recorded from 77 *Sst* neurons, and ~35% (28 of 77) of the tdTomato-labeled neurons were strongly activated by optogenetic stimulation of GCbt projections in the rNST (Figures 6E and S6B–S6K). As would be expected for excitatory input, these responses were blocked by the AMPA (α-amino-3-hydroxy-5-methyl-4-isoxazolepropionic acid) receptor antagonist DNQX (6,7-dinitroquinoxaline-2,3-dione) (Honoré et al., 1988; Figures 6D and 6E). Of note, a fraction of these rNST Sst^+ neurons (7 of 28) also exhibited inhibitory currents that were blocked by TTX (tetrodotoxin) (Narahashi et al., 1964; Figures S6G–S6L), demonstrating that they were mediated via activation of inhibitory interneurons; these inhibitory inputs likely help maintain the excitation/inhibition balance and prevent potential runaway feedforward excitation (Isaacson and Scanziani, 2011).

To directly validate the top-down monosynaptic connections between the bitter taste cortex (GCbt) and *Sst* neurons in the brainstem, we used a retrograde viral tracer (Figure S7A). In essence, we infected the rNST of *Sst-cre* animals with a cocktail of AAV viruses harboring a Cre-dependent viral receptor (TVA [avian tumor virus receptor A]) to restrict infection of the transsynaptic viral tracer to Sst^+ neurons, a glycoprotein coat gene (G) required for viral packaging and transfer (to limit transsynaptic transfer monosynaptically), and red fluorescent reporters (mKate/mCherry) (Reardon et al., 2016; Wickersham et al., 2007a, 2007b). Two weeks after the initial infection, the rNST was infected with the retrograde RABV-ΔG-GFP rabies virus. Our results (Figure S7B) showed efficient transfer of the rabies reporter from the rNST to the GCbt, confirming the monosynaptic connections between GCbt neurons in the cortex and *Sst* bitter neurons in the rNST.

Next we studied the basis for bitter-mediated suppression of *Calb2* sweet neurons. We performed similar recording experiments using brainstem slices with *Calb2* sweet neurons labeled with tdTomato and GCbt projections expressing ChR2-YFP. Surprisingly, we found no significant numbers of *Calb2* neurons that received input from the GCbt (only 1 of 23 cells in 5 animals showed excitatory input from the GCbt; data not shown). We hypothesized that the GCbt may exert its modulation on sweet neurons in the rNST via the amygdala (the CeA and its projections to the rNST, as shown in Figures 1C and 1D; Wang et al., 2018). Thus, we engineered animals expressing ChR2 in the CeA and recorded from tdTomato-labeled *Calb2* sweet neurons (Figure 6F). We patched 11 *Calb2* sweet neurons from multiple animals, and, indeed, every one exhibited a strong inhibitory response following optogenetic activation of the CeA→ rNST projections (Figures 6G–6I). As expected, these responses were blocked by the GABA receptor blocker PTX (picrotoxin) (Newland and Cull-Candy, 1992) but were unaffected by DNQX, substantiating their inhibitory nature (Figures 6H and 6I). To validate the monosynaptic connections between CeA and *Calb2* neurons in the rNST, we also carried out retrograde viral tracing experiments (Figure S7C).

Finally, to demonstrate that the amygdala-evoked suppression indeed originates *in vivo* in the GCbt (via its major projections to the CeA; Wang et al., 2018), we implanted stimulating optical

Figure 3. Ablation of Sweet and Bitter Neurons in the rNST Abolishes Aversion to Bitter and Attraction to Sweet

(A) Schematic of a taste preference assay; animals were injected bilaterally with a Cre-dependent DTA virus in the rNST (Figures S3B–S3D) and exposed to sessions of 60 trials of random presentations of various taste stimuli.

(B) Representative histograms illustrating licking events during a 5-s trial of water (gray), 20 mM CA (sour, blue), or 1 mM Qui (bitter, red). The Qui trials have been sorted in the left panel.

(C) Representative histograms (from the same animal as in B) after DTA-mediated ablation of *Sst* neurons in the rNST. Note the selective loss of aversion to bitter stimuli. The dotted line represents average licking responses of control animals to the bitter tastant.

(D) Quantification of lick responses to bitter stimuli (1 mM and 5 mM Qui) before and after ablation of *Sst* neurons (n = 6 mice). Note that *Sst*-ablated animals exhibit no aversion even to exceedingly high concentrations of bitter stimuli. Values are means ± SEM. Paired t tests, $p < 0.0001$ (1 mM and 5 mM Qui).

(E) Responses to sweet and sour are unaffected. n = 6 animals; values are means ± SEM, paired t tests, $p > 0.2$ (AceK), $p > 0.1$ (CA).

(F) Quantification of lick responses to sweet stimuli (4 mM and 20 mM AceK) before and after ablation of *Calb2* neurons (n = 6 mice). *Calb2*-ablated animals exhibit a dramatically reduced preference for sweet stimuli (red bars). Values are means ± SEM. Paired t tests, $p < 0.001$ (4 mM AceK), $p < 0.005$ (20 mM AceK).

(G) Lick responses to salt (100 mM NaCl), bitter (1 mM Qui), and sour (20 mM CA) are unaffected. n = 6 animals; values are means ± SEM, paired t tests, $p > 0.9$ (NaCl), $p > 0.6$ (Qui), $p > 0.1$ (CA).

(H) We also assayed the sweet preference of *Calb2*-ablated animals using a long-term sweet preference test (water versus sweet over a 24-h period). Ablation of *Calb2* neurons in the rNST completely abolished sweet preference in a standard two-bottle preference assay, even when using extremely high concentrations of sweetener (red bars). Ratio refers to volume of sweet versus water consumed over the 24-h session. Gray bars, control animals injected with Flex-DTA (n = 4); red bars, *Calb2-cre* animals injected with Flex-DTA (n = 6). Values are means ± SEM; unpaired t tests, $p < 0.05$ (1.5 mM AceK), $p < 0.0001$ (20 mM AceK).

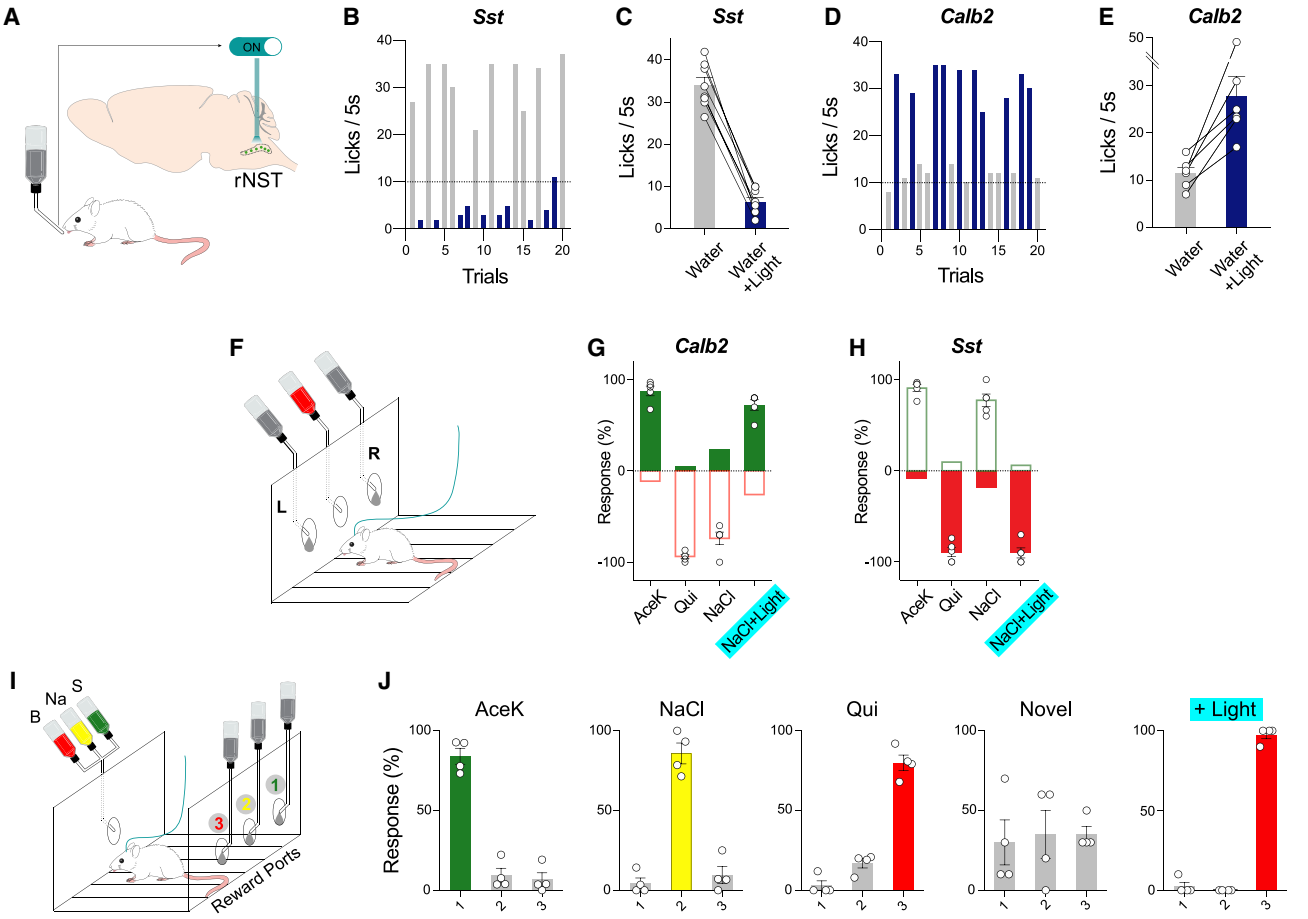

Figure 4. Activation of *Sst* and *Calb2* Neurons in the rNST Mimics Bitter and Sweet Tastes

(A) Schematic of the lick-triggered optogenetic stimulation strategy. *Sst* or *Calb2* neurons were transduced with Cre-dependent AAV-Flex-ChR2, and a stimulating optic fiber was placed above the rNST. Photo-stimulation was triggered by the animal's licking.

(B) Representative histograms of licking events with (blue) or without (gray) photo-stimulation. Note that activation of *Sst* neurons markedly suppressed licking.

(C) Quantification of lick responses; n = 8 animals. Values are means ± SEM; paired t test, $p < 0.0001$.

(D) Representative histograms of licking events with (blue) or without (gray) light stimulation. Note that activation of *Calb2* neurons markedly enhanced licking.

(E) Quantification of lick responses; n = 6 animals. Values are means ± SEM; paired t test, $p = 0.01$.

(F) Schematic illustrating the three-port taste recognition task. The animals were trained to sample a randomly chosen tastant from the center spout and report its identity by going to the left or right port (see STAR Methods for details).

(G) Summary graph showing that animals reliably identified sweet (4 mM AceK), bitter (1 mM Qui), and low salt (3 mM NaCl). Importantly, they cross-generalize between sweet stimuli and optogenetic stimulation of *Calb2* neurons; n = 5 animals. Values are means ± SEM; one-way ANOVA followed by Tukey post hoc test, $p < 0.001$ (NaCl versus light), $p > 0.3$ (light versus AceK).

(H) Summary graph demonstrating that animals cross-generalized between bitter stimuli and optogenetic stimulation of *Sst* neurons; n = 5 animals. Values are means ± SEM. One-way ANOVA followed by Tukey post hoc test, $p < 0.001$ (NaCl versus light), $p > 0.9$ (light versus Qui).

(I) Schematic illustrating the four-port taste recognition task. Animals were trained to lick a randomly presented tastant from the sampling spout and report its identity by subsequently choosing one of the three response ports for a water reward (port 1, 2, or 3). Correct answers were rewarded with 5 s of water, whereas incorrect ones received a 5-s time out (see STAR Methods for details).

(J) Summary graph showing that animals reliably identified sweet (4 mM AceK), bitter (1 mM Qui), and salty (60 mM NaCl). In contrast, the animals responded randomly among the three reward ports when given a novel stimulus (3 mM NaCl). Optogenetic stimulation of *Sst* neurons is recognized as a bitter stimulus (port 3), demonstrating the cross-generalization between bitter and activation of *Sst* neurons; n = 4 animals. Values are means ± SEM; one-way ANOVA followed by Tukey post hoc test, $p < 0.01$ (novel versus light), $p = 0.17$ (light versus Qui).

fibers over the amygdala of mice expressing ChR2 in the GCbt and assayed whether ChR2 activation of GCbt-to-CeA projections suppresses the sweet-evoked activity in *Calb2* neurons. As predicted, optogenetic activation of GCbt terminals in the CeA re-capitulated the strong inhibition of *Calb2* sweet neurons observed when directly stimulating the GCbt (Figure 5E). Not surprisingly, stimulation of GCbt projections to the CeA had no effect on the activity of *Sst* bitter neurons in the rNST (Figure 5F). These results explain the cellular and physiological basis for the positive and negative feedback from the bitter taste cortex: direct

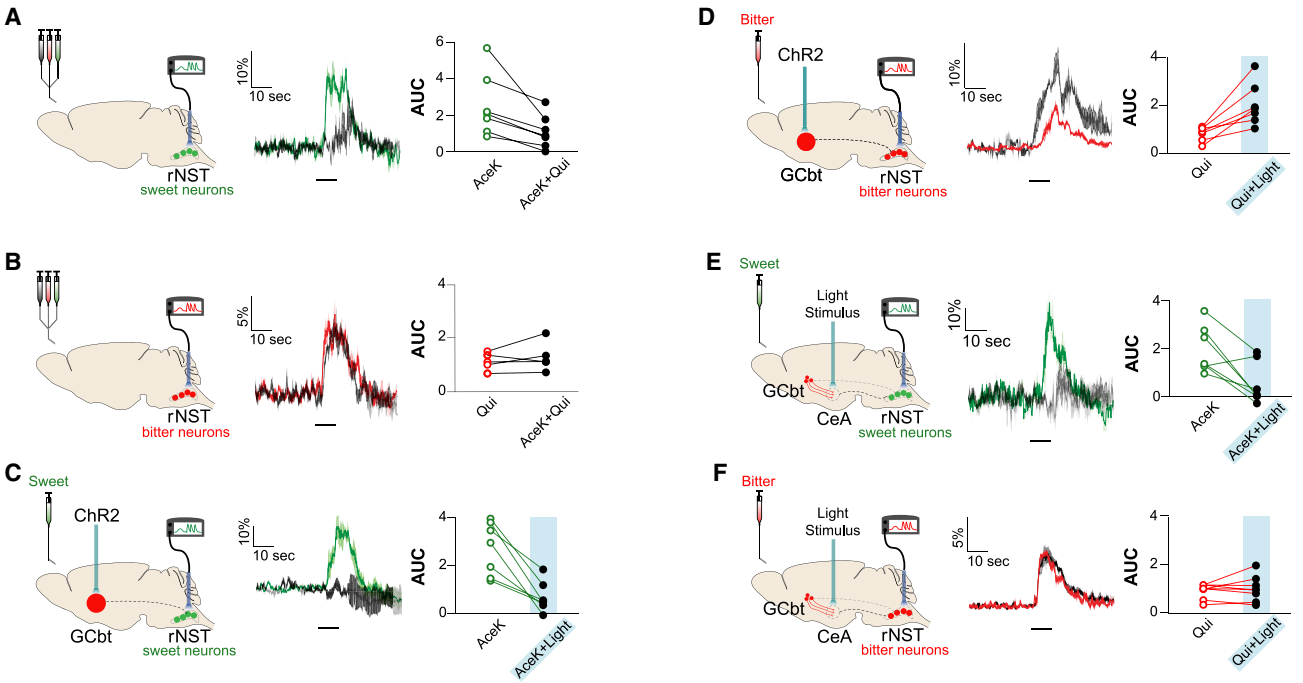

Figure 5. Feedback Modulation of Sweet and Bitter Neurons in the rNST

(A) Responses of *Calb2* neurons to a sweet or sweet and bitter mix. The presence of the bitter tastant strongly suppressed sweet-evoked activity. The green trace shows a sample recording of the sweet-alone stimulus (4 mM AceK) and the black trace the response to the mix (4 mM AceK plus 5 mM Qui); the black bar denotes the duration of the taste stimulus (10 s). Scale, ΔF/F. The right panel shows quantitation; n = 7 animals; paired t test, p = 0.01.

(B) Responses of *Sst* neurons to a bitter or sweet and bitter mix. The presence of the sweet tastant has no significant effect on the bitter-evoked activity of *Sst* neurons, even when using extremely high concentrations of the sweet tastant. The red trace shows the response to the bitter-alone stimulus (1 mM Qui) and the black trace the response to the mix (20 mM AceK plus 1 mM Qui). The right panel shows quantitation of the responses; n = 5 animals; paired t test, p > 0.3.

(C) Activation of the GCbt suppresses the sweet responses of *Calb2* neurons. Neurons in the GCbt were transduced with an AAV-CaMKII-ChR2 virus (Peng et al., 2015), and a stimulating fiber (ChR2) was placed over the GCbt (red). The same animals expressed GCaMP6s in *Calb2* neurons in the rNST. The center panel shows a sample recording illustrating dramatic inhibition of sweet-evoked signals. The green trace shows the response to 4 mM AceK and the black trace the response to 4 mM AceK with stimulation of the GCbt (see also Figure S5B). Scale, ΔF/F. The right panel shows quantitation of the responses; n = 7 animals. Paired t test, p = 0.001. The black bars under the traces in (C)–(F) denote the duration of taste and light stimuli (10 s).

(D) Activation of the GCbt enhances the response of *Sst* neurons to a bitter stimulus. The red trace shows a sample recording to a 1 mM Qui stimulus and the black trace the response to the same stimulus paired with stimulation of the GCbt; n = 7 animals. Paired t test, p = 0.005. See also Figure S5A.

(E) Optogenetic stimulation of the projections from bitter cortical neurons to the CeA is sufficient to suppress the response of *Calb2* neurons to a sweet tastant. The GCbt was transduced with an AAV-CaMKII-ChR2 virus, but the photo-stimulation fiber was placed above the CeA (Wang et al., 2018). The same animals expressed GCaMP6s in *Calb2* neurons in the rNST. The center panel shows a sample recording illustrating inhibition of sweet-evoked signals. The green trace shows the response to a 4 mM AceK stimulus and the black trace the response to the same stimulus when paired with co-stimulation of GCbt terminals in the CeA; n = 7 animals. Paired t test, p = 0.01. See also Figure S5C.

(F) Activation of the projections of bitter cortical neurons in the CeA has no effect on the responses of *Sst* neurons to a bitter stimulus; compare and contrast with (D). The red trace shows a sample response to 1 mM Qui and the black trace the response to 1 mM Qui with stimulation of bitter terminals in the CeA; n = 8 animals. Paired t test, p > 0.5.

In all experiments, taste stimuli were delivered through intra-oral infusion in awake animals (see STAR Methods for details).

excitatory input from the GCbt onto bitter brainstem neurons to enhance incoming bitter signals and inhibitory input via the CeA to concomitantly suppress the activity of the incoming sweet signals in the brainstem.

Silencing Top-Down Modulation Abolishes Bitter-Evoked Sweet Suppression

A key prediction of our results is that if the CeA to rNST negative feedback indeed mediates bitter-evoked suppression of incoming sweet signals *in vivo*, then blocking the top-down CeA-to-rNST feedback should abolish bitter-evoked inhibition of sweet signals.

First we pharmacologically silenced the CeA by infusion of the AMPA receptor antagonist NBQX (2,3-dioxo-6-nitro-1,2,3,4-tetrahydrobenzo[f]quinoxaline-7-sulfonamide) (Tye et al., 2011). We implanted cannulas bilaterally into the CeA, waited 2 weeks for recovery, and assayed the responses of *Calb2* neurons in the rNST before and after bilateral injection of NBQX (Figure 7A). Indeed, our results (Figure 7B) showed that *Calb2* sweet responses are no longer suppressed by the presence of a bitter stimulus. As expected, loss of sweet suppression is fully reversible upon washout of the drug (Figure 7B). Next we examined the effect of CeA inhibition on behavior. We used a behavioral test where animals were exposed to drinking sessions consisting of

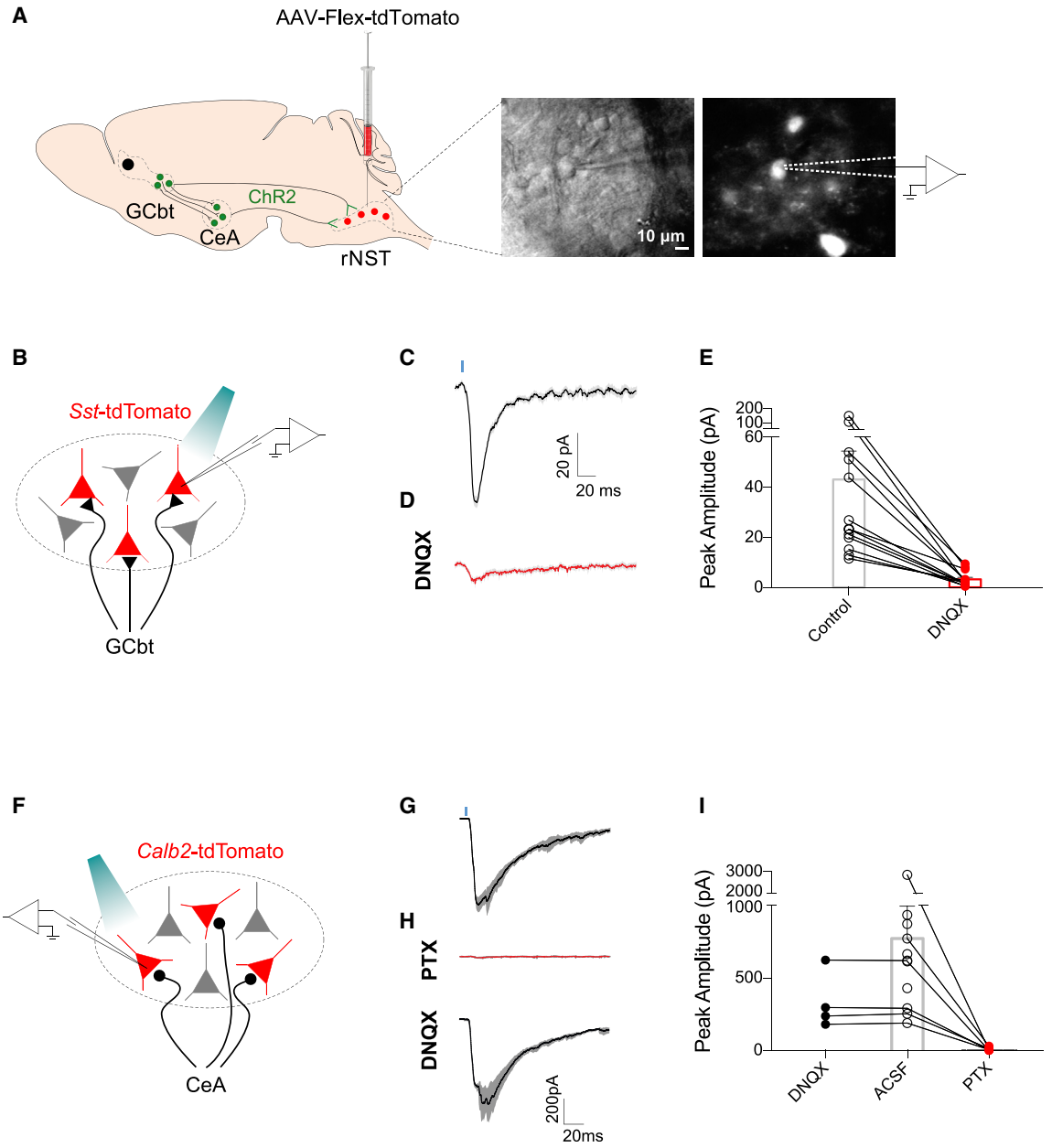

Figure 6. Top-Down Synaptic Excitation and Inhibition of *Sst* and *Calb2* Neurons

(A) ChR2 was targeted to the bitter cortical neurons (GCbt) or CeA neurons, and a Cre-dependent tdTomato (AAV-Flex-tdT) reporter virus was injected into the rNST to mark *Sst*- or *Calb2*-expressing neurons. The diagram shows the strategy for channelrhodopsin-2 (ChR2)-assisted patch-clamp mapping of the synaptic connections between projections from the GCbt and CeA and the sweet and bitter neurons in the rNST slice preparation (right micrograph). The fluorescently labeled neurons were recorded in whole-cell voltage-clamp mode; dashed lines outline the patching pipette (see also Figure S6A).

(B) Schematic of whole-cell patch-clamp recording of postsynaptic currents in *Sst*-expressing neurons in the rNST while optogenetically activating bitter cortical terminals.

(C) Light activation of ChR2$^+$ in bitter cortical terminals in the rNST triggered time-locked excitatory postsynaptic currents (EPSCs) in *Sst*-expressing neurons. The sample traces show average responses ± SEM; for additional traces, see Figure S6C. The monosynaptic nature of EPSCs was inferred by the short onset latency (<15 ms) and verified by their insensitivity to TTX (tetrodotoxin) and 4-AP (4-aminopyridine) (Figure S6F) and retrograde labeling experiments (Figure S7).

(D) These EPSCs are completely blocked by the AMPA receptor blocker DNQX (red trace). The blue bar denotes the onset and duration of the light stimulus.

(E) Quantification of EPSC responses. Shown are peak amplitudes (n = 13 neurons from 6 animals) that exhibited activation following optogenetic stimulation of bitter cortical terminals; responses from all 13 were blocked by DNQX (solid red circles) (see also Figures S6D and S6E). Values are means ± SEM.

(F) Schematic of whole-cell patch-clamp recording of postsynaptic currents in *Calb2*-expressing neurons in the rNST with optogenetic activation of CeA terminals in the rNST slice.

(G) Light activation of ChR2$^+$ in CeA terminals in the rNST triggered time-locked inhibitory postsynaptic currents (IPSCs) in *Calb2*-expressing neurons.

(legend continued on next page)

random presentations of bitter, sweet, or the sweet-bitter mix (Figure 7C). Prior to pharmacological silencing, mice exhibited reduced licking to bitter stimuli, strong licking responses to sweet stimuli, and greatly reduced licking to the sweet-bitter mix (Figure 7D). However, after silencing, the animals showed a dramatic increase in attraction to the sweet-bitter mix (Figure 7D). Importantly, this behavioral change is fully reversible upon washout of the drug, whereas injection of a saline control in the CeA had no significant effect on the responses to any of the tastants (Figure 7D).

To directly demonstrate that the CeA-to-rNST projections drive bitter-evoked suppression of incoming sweet signals, we carried out photoinhibition experiments. We infected the CeA with AAVs harboring inhibitory opsins (Guillardia theta anion channel rhodopsin 1 [GtACR1] or enhanced halorhodopsin [eNpHR]) (Govorunova et al., 2015; Gradinaru et al., 2010) and placed the stimulating optical light fiber in the CeA projections to the rNST (Figure 7E, CeA → rNST); we utilized two different inhibitory opsins to minimize potential confounds arising from use of a single silencing strategy (Wiegert et al., 2017). We used a behavioral test where head-attached, motivated animals (i.e., thirsty) were trained to sample random presentations of 3 different stimuli: sweet, bitter, and the sweet-bitter mix. We then subjected the animals to sessions consisting of a series of trials, but in a fraction of the trials, the CeA-to-rNST projections were optogenetically silenced. Figure 7F demonstrates that silencing negative feedback from the CeA to the rNST strongly relieves bitter-evoked suppression to a bitter-sweet mix with no significant effect on responses to sweet- or bitter-alone stimuli. In contrast, light stimulation of CeA→rNST projections that expressed a control GFP had no effect (Figure 7G). These pharmacological and optogenetic silencing studies validate the key role of the top-down inhibition in modulating responses to taste mixes of sweet-bitter stimuli. We note that, although the imperfect effect of the inhibitory opsins could be due to the inherent inefficiency of bilateral silencing, it may also be a reflection of additional bitter-evoked suppressing mechanisms, such as a local inhibitory circuit in the rNST (Thek et al., 2019).

DISCUSSION

Hardwired circuits and behaviors have been a prominent feature of lower organisms and have generally been viewed as encoding simple actions in the mammalian brain. In contrast, more complex behaviors have been thought to be primarily learned. However, this perspective has changed significantly as multifaceted behavioral (Peng et al., 2015), metabolic (Münzberg et al., 2016), and physiological (Zimmerman et al., 2017) responses have been found to be mediated by hardwired circuits.

The taste system functions as the primary gate controlling feeding choices and consummatory behaviors and has emerged as one of the most salient examples of a multi-stage hardwired circuit in the mammalian brain. Previously, we showed that the sense of taste operates via labeled lines wired to trigger stereotyped behaviors (Lee et al., 2017; Mueller et al., 2005; Zhao et al., 2003), requiring no prior learning or experience (Peng et al., 2015). For example, direct stimulation of the sweet or bitter (GCbt) cortical fields elicits entire behavioral programs normally evoked by orally applied sweet or bitter tastants. Most critically, however, optogenetic activation of the taste cortex also elicits the same taste responses in animals that have never experienced the "taste" of sweet or bitter (because of genetic removal of an essential taste-signaling component in TRCs; Peng et al., 2015), confirming the predetermined nature of the sense of taste.

Here we showed that the hardwired neurons for sweet and bitter can be intermingled with each other without affecting their labeled-line properties, formally disentangling the concept and logic of labeled-line coding from topography; i.e., taste neurons can be segregated (Chen et al., 2011; see also Figure S7) or intermingled independent of their single-taste coding properties.

We revealed how top-down control from the cortex can exert exquisite control over hardwired behaviors (Liang et al., 2015; Liu et al., 2016; Xiong et al., 2015). Our results illustrate how the taste system uses dedicated feedback lines to modulate innate behavioral responses. The circuit logic is simple and elegant: to provide directed, opposing feedback that enhances behavioral aversion while suppressing attraction. Importantly, both act at the brainstem, the key nexus of signal propagation from the periphery into the brain, affording a powerful solution to ensuring bitter aversion in the mammalian taste system. This differs from insects like *Drosophila*, where the interaction between sweet and bitter signals takes place at the earlier stages, including at the sensory neuron level (French et al., 2015; Harris et al., 2015; Jeong et al., 2013) or presynaptically before the second-order neurons (Chu et al., 2014).

Do bitter signals in the rNST also locally inhibit *Calb2* sweet neurons? The finding that suppression of sweet signals is dramatically weakened after blocking top-down negative feedback (Figure 7) strongly argues that inhibition of incoming sweet signals (i.e., from the tongue to the rNST) is primarily initiated by CeA negative feedback. However, it is possible that a local inhibitory network in the brainstem may be activated by ascending bitter signals on their way to the cortex. At an evolutionary level, it would be advantageous to have multiple mechanisms ensuring suppression of sweet attraction by bitter signals.

The insular cortex, in addition to being a gustatory area, is also an important interoceptive site, integrating multisensory signals with the internal state (Saper, 2002). Interestingly, a number of studies have shown that behavioral repulsion to aversive tastes can be overcome by association with a strong positive reinforcer, such as alcohol (Seif et al., 2013; Siciliano et al., 2019). In the future, it will be of interest to examine how the various taste stations in the brain interact and are modulated by each other

(H) These IPSCs are irreversibly blocked by the GABA receptor antagonist PTX but not affected by DNQX.
(I) Quantification of IPSC responses; shown are peak amplitudes. n = 11 neurons (from 4 animals), and all 11 responded to optogenetic stimulation of CeA terminals. The solid black circles demonstrate that the IPSCs are unaffected by the AMPA receptor blocker DNQX (4 of 4 tested neurons). In contrast, they are irreversibly blocked by the GABA receptor antagonist PTX (6 of 6 tested neurons, solid red circles). Values are means ± SEM. Additional traces and quantifications are shown in in Figures S6M–S6P.

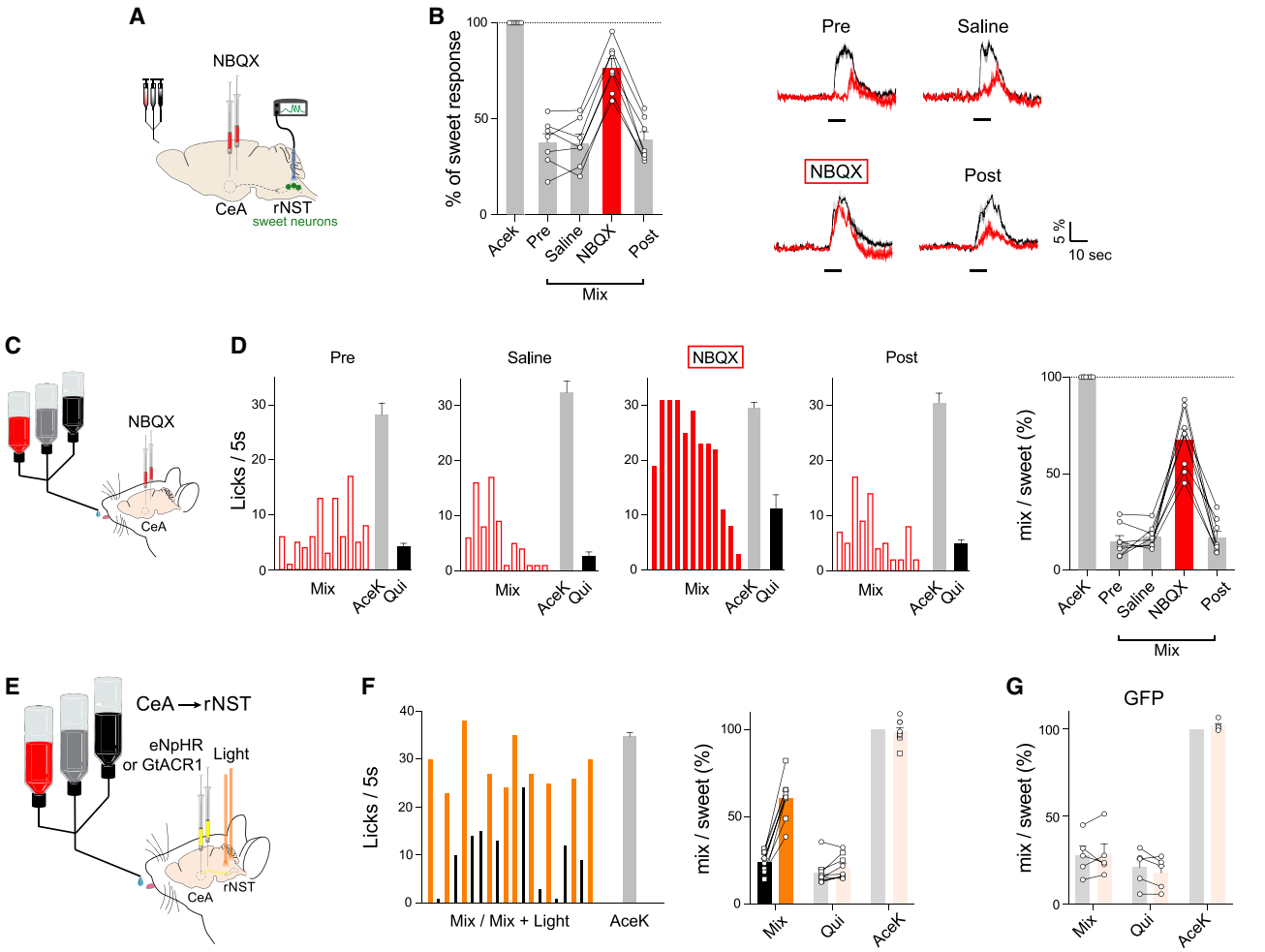

Figure 7. Silencing Inhibitory Feedback

(A) Schematic of the pharmacological silencing strategy. Mice were implanted bilaterally with cannulas for infusion of NBQX in the CeA. A Cre-dependent GCaMP6s reporter (AAV-Flex-GCaMP6s) was targeted to *Calb2* sweet neurons in the rNST, and head-attached, awake animals were stimulated intra-orally with sweet and sweet-bitter stimuli before, during, and after NBQX treatment.

(B) Pharmacological silencing of CeA suppresses bitter-evoked inhibition of sweet responses. The traces shown are sample average responses (solid color traces) ± SEM (shade) to a sweet-alone stimulus (10 mM AceK, black) and a sweet-bitter mix (10 mM AceK + 2 mM Qui, red) before infusion (pre) and after infusion of saline or NBQX. Also shown are responses after washout of the drug (post). The left panel shows quantification; responses were normalized to sweet alone from the same recording session. n = 7 mice; values are means ± SEM; one-way ANOVA followed by Tukey post hoc test, $p = 1$ (saline versus pre), $p < 0.0001$ (NBQX versus pre), $p < 0.0001$ (NBQX versus saline). For sweet alone, the graph shows responses before infusion.

(C) NBQX silencing of the CeA abolishes behavioral aversion to sweet-bitter mixtures. Cannulas were implanted bilaterally over the CeA for pharmacological silencing, and mice were tested for taste responses to sweet, bitter, and sweet-bitter stimuli.

(D) Representative histograms showing licking events in response to 5 s of sweet (10 mM AceK, gray), bitter (2 mM Qui, black), or a sweet-bitter mix (10 mM AceK plus 2 mM Qui, red). The 4 panels show responses (sorted) before infusion (pre), after infusion of saline and NBQX, and after washout of the drug (post). The AceK and Qui trials are shown as mean ± SEM. The right panel shows quantification; lick counts were normalized to sweet alone for each recording session. n = 8 mice, values are means ± SEM; one-way ANOVA followed by Tukey post hoc test, $p > 0.8$ (saline versus pre), $p = 0.0002$ (NBQX versus pre); $p = 0.0004$ (NBQX versus saline). The small increase in licks to bitter stimuli after NBQX inhibition of the CeA (Wang et al., 2018) is not seen when using more selective optogenetic inhibition of the CeA projections to the rNST (E and F).

(E) Schematic of the photoinhibition strategy. Inhibitory opsins, eNpHR3.0 or GtACR1, were injected bilaterally into the CeA, and stimulating fibers were placed bilaterally above the rNST to silence CeA terminals in the rNST. The animals were tested for licking responses to sweet, bitter, and a sweet-bitter mix with and without photoinhibition.

(F) Silencing CeA-to-rNST projection markedly suppresses aversion to a sweet-bitter mixture. Shown are representative histograms illustrating licking events to 5-s stimuli of a sweet-bitter mix (10 mM AceK + 2 mM Qui) in the absence (black) or presence of photostimulation (orange); lick counts were normalized to sweet alone (without photostimulation) for each recording session. The right panel shows quantification. n = 9 mice (4 animals with eNpHR3.0 [open circles] and 5 animals with GtACR1 [open squares]); values are means ± SEM, paired t tests: mix versus mix + light, $p < 0.0001$; Qui versus Qui + light, $p = 0.06$; AceK versus AceK + light, $p > 0.5$. Note that photoinhibition had no significant effect on the responses to sweet- or bitter-alone stimuli.

(legend continued on next page)

and by internal state signals, like reward, nutritional needs, hunger, satiety, emotion, and expectation, to alter taste perception and taste-related behaviors.

STAR★METHODS

Detailed methods are provided in the online version of this paper and include the following:

- KEY RESOURCES TABLE
- RESOURCE AVAILABILITY
  - Lead Contact
  - Materials Availability
  - Data and Code Availability
- EXPERIMENTAL MODEL AND SUBJECT DETAILS
  - Animals
- METHOD DETAILS
  - Viral constructs
  - Stereotaxic surgery
  - Intraoral fistula implantation
  - Head-attached licking preference assay
  - Freely moving licking preference assay
  - Two-bottle preference assay
  - Three-port and four-port taste discrimination task
  - DTA mediated cell ablation
  - Photostimulation
  - Infusion and lick fiber photometry
  - Pharmacological Inhibition
  - Whole brain clearing
  - Brain slice electrophysiological recordings
  - Monosynaptic retrograde tracing
  - Histology
- QUANTIFICATION AND STATISTICAL ANALYSIS

ACKNOWLEDGMENTS

We thank the Zuckerman Institute's Cellular Imaging platform for help with CUBIC. We particularly thank members of the Zuker lab for helpful discussions and Nick Ryba for helpful suggestions. We also thank Kimberly Ritola from the Janelia Research Campus Viral Core for help with viral constructs and production; Minmin Luo from the National Institute of Biological Sciences, Beijing for providing the AAV-GtACR1 viral construct; and Zaiqi Wu for help with animal constructs. We are also grateful to Laura Rickman for expert help with the figures. Z.H.F. was supported by a National Science Foundation, USA pre-doctoral graduate research fellowship. Research reported in this publication was supported in part by the Russell Berrie Foundation program in the neurobiology of obesity (to C.S.Z. and Rudy Leibel). C.S.Z. is an investigator of the Howard Hughes Medical Institute. Figures were generated with the help of BioRender.

AUTHOR CONTRIBUTIONS

H.J. and Z.H.F. designed the study, carried out the experiments, and analyzed data. M.Y. designed the study, implemented the slice preparation, carried out patch-clamp and optogenetic recordings, and analyzed data. L.W. carried out imaging experiments using light-sheet microscopy, designed experiments, and analyzed data. C.S.Z. designed the study and analyzed data, and C.S.Z., H.J., and Z.H.F. wrote the paper.

DECLARATION OF INTERESTS

The authors declare no competing interests.

Received: January 10, 2020
Revised: July 20, 2020
Accepted: December 9, 2020
Published: January 7, 2021

REFERENCES

Anderson, D.J. (2016). Circuit modules linking internal states and social behaviour in flies and mice. Nat. Rev. Neurosci. *17*, 692–704.

Antinucci, M., and Risso, D. (2017). A Matter of Taste: Lineage-Specific Loss of Function of Taste Receptor Genes in Vertebrates. Front. Mol. Biosci. *4*, 81.

Bales, M.B., Schier, L.A., Blonde, G.D., and Spector, A.C. (2015). Extensive Gustatory Cortex Lesions Significantly Impair Taste Sensitivity to KCl and Quinine but Not to Sucrose in Rats. PLoS ONE *10*, e0143419.

Barretto, R.P., Gillis-Smith, S., Chandrashekar, J., Yarmolinsky, D.A., Schnitzer, M.J., Ryba, N.J., and Zuker, C.S. (2015). The neural representation of taste quality at the periphery. Nature *517*, 373–376.

Blonde, G.D., Bales, M.B., and Spector, A.C. (2015). Extensive lesions in rat insular cortex significantly disrupt taste sensitivity to NaCl and KCl and slow salt discrimination learning. PLoS ONE *10*, e0117515.

Boyden, E.S., Zhang, F., Bamberg, E., Nagel, G., and Deisseroth, K. (2005). Millisecond-timescale, genetically targeted optical control of neural activity. Nat. Neurosci. *8*, 1263–1268.

Chandrashekar, J., Kuhn, C., Oka, Y., Yarmolinsky, D.A., Hummler, E., Ryba, N.J., and Zuker, C.S. (2010). The cells and peripheral representation of sodium taste in mice. Nature *464*, 297–301.

Chen, X., Gabitto, M., Peng, Y., Ryba, N.J., and Zuker, C.S. (2011). A gustotopic map of taste qualities in the mammalian brain. Science *333*, 1262–1266.

Chen, T.W., Wardill, T.J., Sun, Y., Pulver, S.R., Renninger, S.L., Baohan, A., Schreiter, E.R., Kerr, R.A., Orger, M.B., Jayaraman, V., et al. (2013). Ultrasensitive fluorescent proteins for imaging neuronal activity. Nature *499*, 295–300.

Chu, B., Chui, V., Mann, K., and Gordon, M.D. (2014). Presynaptic gain control drives sweet and bitter taste integration in Drosophila. Curr. Biol. *24*, 1978–1984.

Damak, S., Rong, M., Yasumatsu, K., Kokrashvili, Z., Pérez, C.A., Shigemura, N., Yoshida, R., Mosinger, B., Jr., Glendinning, J.I., Ninomiya, Y., and Margolskee, R.F. (2006). Trpm5 null mice respond to bitter, sweet, and umami compounds. Chem. Senses *31*, 253–264.

Dong, D., Jones, G., and Zhang, S. (2009). Dynamic evolution of bitter taste receptor genes in vertebrates. BMC Evol. Biol. *9*, 12.

French, A.S., Sellier, M.J., Ali Agha, M., Guigue, A., Chabaud, M.A., Reeb, P.D., Mitra, A., Grau, Y., Soustelle, L., and Marion-Poll, F. (2015). Dual mechanism for bitter avoidance in Drosophila. J. Neurosci. *35*, 3990–4004.

Glendinning, J.I., Gresack, J., and Spector, A.C. (2002). A high-throughput screening procedure for identifying mice with aberrant taste and oromotor function. Chem. Senses *27*, 461–474.

Govorunova, E.G., Sineshchekov, O.A., Janz, R., Liu, X., and Spudich, J.L. (2015). Natural light-gated anion channels: A family of microbial rhodopsins for advanced optogenetics. Science *349*, 647–650.

(G) Control wild-type animals were injected bilaterally into the CeA with AAV-GFP, and stimulating fibers were placed bilaterally above the rNST. Shown is quantification of licking events to 5-s stimuli of a sweet-bitter mix (10 mM AceK + 2 mM Qui), bitter alone (2 mM Qui), and sweet alone (10 mM AceK). n = 5 mice; values are means ± SEM, paired t tests: mix versus mix + light, $p > 0.9$; Qui versus Qui + light, $p = 0.16$; AceK versus AceK + light, $p > 0.2$.

Gradinaru, V., Zhang, F., Ramakrishnan, C., Mattis, J., Prakash, R., Diester, I., Goshen, I., Thompson, K.R., and Deisseroth, K. (2010). Molecular and cellular approaches for diversifying and extending optogenetics. Cell *141*, 154–165.

Gunaydin, L.A., Grosenick, L., Finkelstein, J.C., Kauvar, I.V., Fenno, L.E., Adhikari, A., Lammel, S., Mirzabekov, J.J., Airan, R.D., Zalocusky, K.A., et al. (2014). Natural neural projection dynamics underlying social behavior. Cell *157*, 1535–1551.

Hardaway, J.A., Halladay, L.R., Mazzone, C.M., Pati, D., Bloodgood, D.W., Kim, M., Jensen, J., DiBerto, J.F., Boyt, K.M., Shiddapur, A., et al. (2019). Central Amygdala Prepronociceptin-Expressing Neurons Mediate Palatable Food Consumption and Reward. Neuron *102*, 1088.

Harris, D.T., Kallman, B.R., Mullaney, B.C., and Scott, K. (2015). Representations of Taste Modality in the Drosophila Brain. Neuron *86*, 1449–1460.

Hayama, T., and Ogawa, H. (2001). Two loci of the insular cortex project to the taste zone of the nucleus of the solitary tract in rats. Neurosci. Lett. *303*, 49–52.

He, M., Tucciarone, J., Lee, S., Nigro, M.J., Kim, Y., Levine, J.M., Kelly, S.M., Krugikov, I., Wu, P., Chen, Y., et al. (2016). Strategies and Tools for Combinatorial Targeting of GABAergic Neurons in Mouse Cerebral Cortex. Neuron *92*, 555.

Honoré, T., Davies, S.N., Drejer, J., Fletcher, E.J., Jacobsen, P., Lodge, D., and Nielsen, F.E. (1988). Quinoxalinediones: potent competitive non-NMDA glutamate receptor antagonists. Science *241*, 701–703.

Isaacson, J.S., and Scanziani, M. (2011). How inhibition shapes cortical activity. Neuron *72*, 231–243.

Jeong, Y.T., Shim, J., Oh, S.R., Yoon, H.I., Kim, C.H., Moon, S.J., and Montell, C. (2013). An odorant-binding protein required for suppression of sweet taste by bitter chemicals. Neuron *79*, 725–737.

Krashes, M.J., Shah, B.P., Madara, J.C., Olson, D.P., Strochlic, D.E., Garfield, A.S., Vong, L., Pei, H., Watabe-Uchida, M., Uchida, N., et al. (2014). An excitatory paraventricular nucleus to AgRP neuron circuit that drives hunger. Nature *507*, 238–242.

Lee, J.H., Durand, R., Gradinaru, V., Zhang, F., Goshen, I., Kim, D.-S., Fenno, L.E., Ramakrishnan, C., and Deisseroth, K. (2010). Global and local fMRI signals driven by neurons defined optogenetically by type and wiring. Nature *465*, 788–792.

Lee, H., Macpherson, L.J., Parada, C.A., Zuker, C.S., and Ryba, N.J.P. (2017). Rewiring the taste system. Nature *548*, 330–333.

Liang, F., Xiong, X.R., Zingg, B., Ji, X.Y., Zhang, L.I., and Tao, H.W. (2015). Sensory Cortical Control of a Visually Induced Arrest Behavior via Corticotectal Projections. Neuron *86*, 755–767.

Liu, B.H., Huberman, A.D., and Scanziani, M. (2016). Cortico-fugal output from visual cortex promotes plasticity of innate motor behaviour. Nature *538*, 383–387.

McLean, J.R., Smith, G.A., Rocha, E.M., Hayes, M.A., Beagan, J.A., Hallett, P.J., and Isacson, O. (2014). Widespread neuron-specific transgene expression in brain and spinal cord following synapsin promoter-driven AAV9 neonatal intracerebroventricular injection. Neurosci. Lett. *576*, 73–78.

Mueller, K.L., Hoon, M.A., Erlenbach, I., Chandrashekar, J., Zuker, C.S., and Ryba, N.J. (2005). The receptors and coding logic for bitter taste. Nature *434*, 225–229.

Münzberg, H., Qualls-Creekmore, E., Berthoud, H.R., Morrison, C.D., and Yu, S. (2016). Neural Control of Energy Expenditure. Handb. Exp. Pharmacol. *233*, 173–194.

Narahashi, T., Moore, J.W., and Scott, W.R. (1964). Tetrodotoxin Blockage of Sodium Conductance Increase in Lobster Giant Axons. J. Gen. Physiol. *47*, 965–974.

Nei, M., Niimura, Y., and Nozawa, M. (2008). The evolution of animal chemosensory receptor gene repertoires: roles of chance and necessity. Nat. Rev. Genet. *9*, 951–963.

Nelson, G., Hoon, M.A., Chandrashekar, J., Zhang, Y., Ryba, N.J., and Zuker, C.S. (2001). Mammalian sweet taste receptors. Cell *106*, 381–390.

Newland, C.F., and Cull-Candy, S.G. (1992). On the mechanism of action of picrotoxin on GABA receptor channels in dissociated sympathetic neurones of the rat. J. Physiol. *447*, 191–213.

Oh, S.W., Harris, J.A., Ng, L., Winslow, B., Cain, N., Mihalas, S., Wang, Q., Lau, C., Kuan, L., Henry, A.M., et al. (2014). A mesoscale connectome of the mouse brain. Nature *508*, 207–214.

Peng, Y., Gillis-Smith, S., Jin, H., Tränkner, D., Ryba, N.J., and Zuker, C.S. (2015). Sweet and bitter taste in the brain of awake behaving animals. Nature *527*, 512–515.

Petreanu, L., Huber, D., Sobczyk, A., and Svoboda, K. (2007). Channelrhodopsin-2-assisted circuit mapping of long-range callosal projections. Nat. Neurosci. *10*, 663–668.

Phillips, M.I., and Norgren, R.E. (1970). A rapid method for permanent implantation of intraoral fistula in rats. Behav. Res. Meth. Instrum. *2*, 124.

Reardon, T.R., Murray, A.J., Turi, G.F., Wirblich, C., Croce, K.R., Schnell, M.J., Jessell, T.M., and Losonczy, A. (2016). Rabies Virus CVS-N2c(ΔG) Strain Enhances Retrograde Synaptic Transfer and Neuronal Viability. Neuron *89*, 711–724.

Root, C.M., Denny, C.A., Hen, R., and Axel, R. (2014). The participation of cortical amygdala in innate, odour-driven behaviour. Nature *515*, 269–273.

Rousseeuw, P.J., and Croux, C. (1993). Alternatives to the median absolute deviation. J. Am. Stat. Assoc. *88*, 1273–1283.

Saper, C.B. (2002). The central autonomic nervous system: conscious visceral perception and autonomic pattern generation. Annu. Rev. Neurosci. *25*, 433–469.

Schoch, S., Cibelli, G., and Thiel, G. (1996). Neuron-specific gene expression of synapsin I. Major role of a negative regulatory mechanism. J. Biol. Chem. *271*, 3317–3323.

Scott, K. (2005). Taste recognition: food for thought. Neuron *48*, 455–464.

Seif, T., Chang, S.J., Simms, J.A., Gibb, S.L., Dadgar, J., Chen, B.T., Harvey, B.K., Ron, D., Messing, R.O., Bonci, A., and Hopf, F.W. (2013). Cortical activation of accumbens hyperpolarization-active NMDARs mediates aversion-resistant alcohol intake. Nat. Neurosci. *16*, 1094–1100.

Siciliano, C.A., Noamany, H., Chang, C.J., Brown, A.R., Chen, X., Leible, D., Lee, J.J., Wang, J., Vernon, A.N., Vander Weele, C.M., et al. (2019). A cortical-brainstem circuit predicts and governs compulsive alcohol drinking. Science *366*, 1008–1012.

Spector, A.C., and Travers, S.P. (2005). The representation of taste quality in the mammalian nervous system. Behav. Cogn. Neurosci. Rev. *4*, 143–191.

Susaki, E.A., Tainaka, K., Perrin, D., Kishino, F., Tawara, T., Watanabe, T.M., Yokoyama, C., Onoe, H., Eguchi, M., Yamaguchi, S., et al. (2014). Whole-brain imaging with single-cell resolution using chemical cocktails and computational analysis. Cell *157*, 726–739.

Susaki, E.A., Tainaka, K., Perrin, D., Yukinaga, H., Kuno, A., and Ueda, H.R. (2015). Advanced CUBIC protocols for whole-brain and whole-body clearing and imaging. Nat. Protoc. *10*, 1709–1727.

Taniguchi, H., He, M., Wu, P., Kim, S., Paik, R., Sugino, K., Kvitsiani, D., Fu, Y., Lu, J., Lin, Y., et al. (2011). A resource of Cre driver lines for genetic targeting of GABAergic neurons in cerebral cortex. Neuron *71*, 995–1013.

Teng, B., Wilson, C.E., Tu, Y.H., Joshi, N.R., Kinnamon, S.C., and Liman, E.R. (2019). Cellular and Neural Responses to Sour Stimuli Require the Proton Channel Otop1. Curr. Biol. *29*, 3647–3656.e5.

Thek, K.R., Ong, S.J.M., Carter, D.C., Bassi, J.K., Allen, A.M., and McDougall, S.J. (2019). Extensive Inhibitory Gating of Viscerosensory Signals by a Sparse Network of Somatostatin Neurons. J. Neurosci. *39*, 8038–8050.

Tye, K.M., Prakash, R., Kim, S.Y., Fenno, L.E., Grosenick, L., Zarabi, H., Thompson, K.R., Gradinaru, V., Ramakrishnan, C., and Deisseroth, K. (2011). Amygdala circuitry mediating reversible and bidirectional control of anxiety. Nature *471*, 358–362.

Wang, L., Gillis-Smith, S., Peng, Y., Zhang, J., Chen, X., Salzman, C.D., Ryba, N.J.P., and Zuker, C.S. (2018). The coding of valence and identity in the mammalian taste system. Nature *558*, 127–131.

Whitehead, M.C., Bergula, A., and Holliday, K. (2000). Forebrain projections to the rostral nucleus of the solitary tract in the hamster. J. Comp. Neurol. *422*, 429–447.

Wickersham, I.R., Finke, S., Conzelmann, K.K., and Callaway, E.M. (2007a). Retrograde neuronal tracing with a deletion-mutant rabies virus. Nat. Methods *4*, 47–49.

Wickersham, I.R., Lyon, D.C., Barnard, R.J., Mori, T., Finke, S., Conzelmann, K.K., Young, J.A., and Callaway, E.M. (2007b). Monosynaptic restriction of transsynaptic tracing from single, genetically targeted neurons. Neuron *53*, 639–647.

Wiegert, J.S., Mahn, M., Prigge, M., Printz, Y., and Yizhar, O. (2017). Silencing Neurons: Tools, Applications, and Experimental Constraints. Neuron *95*, 504–529.

Wu, Z., Autry, A.E., Bergan, J.F., Watabe-Uchida, M., and Dulac, C.G. (2014). Galanin neurons in the medial preoptic area govern parental behaviour. Nature *509*, 325–330.

Xiong, X.R., Liang, F., Zingg, B., Ji, X.Y., Ibrahim, L.A., Tao, H.W., and Zhang, L.I. (2015). Auditory cortex controls sound-driven innate defense behaviour through corticofugal projections to inferior colliculus. Nat. Commun. *6*, 7224.

Yarmolinsky, D.A., Zuker, C.S., and Ryba, N.J. (2009). Common sense about taste: from mammals to insects. Cell *139*, 234–244.

Zhang, Y., Hoon, M.A., Chandrashekar, J., Mueller, K.L., Cook, B., Wu, D., Zuker, C.S., and Ryba, N.J. (2003). Coding of sweet, bitter, and umami tastes: different receptor cells sharing similar signaling pathways. Cell *112*, 293–301.

Zhang, J., Jin, H., Zhang, W., Ding, C., O'Keeffe, S., Ye, M., and Zuker, C.S. (2019). Sour Sensing from the Tongue to the Brain. Cell *179*, 392–402.e15.

Zhao, G.Q., Zhang, Y., Hoon, M.A., Chandrashekar, J., Erlenbach, I., Ryba, N.J., and Zuker, C.S. (2003). The receptors for mammalian sweet and umami taste. Cell *115*, 255–266.

Zimmerman, C.A., Leib, D.E., and Knight, Z.A. (2017). Neural circuits underlying thirst and fluid homeostasis. Nat. Rev. Neurosci. *18*, 459–469.

STAR★METHODS

KEY RESOURCES TABLE

REAGENT or RESOURCE	SOURCE	IDENTIFIER
Antibodies		
Anti-Calb2	immunostar	Cat# 24445; RRID: AB-572223
Bacterial and Virus Strains		
AAV1-Syn-GCaMP6s-WPRE-SV40	Chen et al., 2013	Addgene AAV1; 100843-AAV1
AAV1-Syn-Flex-GCaMP6s-WPRE-SV40	Chen et al., 2013	Addgene AAV1; 100845-AAV1
AAV1-EF1a-DIO-hChR2(H134R)-eYFP-WPRE-hGH	A gift from Karl Deisseroth	Addgene AAV1; 20298-AAV1
AAV9-CaMKIIa-hChR2(H134R)-EYFP	Lee et al., 2010	Addgene AAV9; 26969-AAV9
AAV1-Syn-hChR2(H134R)-EYFP	A gift from Karl Deisseroth	Addgene AAV1; 26973-AAV1
AAV1-hSyn-eNpHR3.0-EYFP	A gift from Karl Deisseroth	Addgene AAV1; 26972-AAV1
AAV1-CMV-PI.EGFP-WPRE-bGH	A gift from James M. Wilson	Addgene AAV1; 105530-AAV1
AAV1-CAG-tdTomato	A gift from Edward Boyden	Addgene AAV1; 59462-AAV1
AAV1-CAG-Flex-tdTomato	Oh et al., 2014	Addgene AAV1; 51502-AAV1
AAV1-CAG-Flex-EGFP	Oh et al., 2014	Addgene AAV1; 51503-AAV1
AAV1-mCherry-Flex-dtA	UNC vector core	N/A
AAV1-EF1a-FLEX-TVAmCherry	UNC vector core	N/A
AAV1-hSyn-Cre	Janelia	N/A
AAV1-CAG-Flex-GtACR1-P2A-EGFP	Janelia	N/A
AAV1-Flex-G(N2C)-mKate	Janelia	N/A
AAV1-fDIO-tdTomato	Janelia	N/A
RABV-N2C(ΔG)-GFP-EnvA	Janelia	N/A
Chemicals, Peptides, and Recombinant Proteins		
Acesulfame K	Sigma-Aldrich	04054
Actidione (Cycloheximide)	Fluka	01810
Citric Acid	Sigma-Aldrich	251275
Quinine monohydrochloride dihydrate	Sigma-Aldrich	145920
Sodium Chloride	Sigma-Aldrich	S5886
Sucrose	Sigma-Aldrich	S9378
DNQX	Sigma-Aldrich	D0540
Picrotoxin	Sigma-Aldrich	P1675
4-Aminopyridine	Sigma-Aldrich	A78403
NBQX disodium salt	Tocris	1044
D-AP5	Tocris	0106
Tetrodotoxin citrate	Tocris	1069
Critical Commercial Assays		
RNAscope Multiplex Fluorescent Detection Kit v2	Advanced Cell diagnostics	323110

(*Continued on next page*)

Continued

REAGENT or RESOURCE	SOURCE	IDENTIFIER
Experimental Models: Organisms/Strains (Mouse)		
C57BL/6J	The Jackson Laboratory	000664
Sst-IRES-Cre	The Jackson Laboratory	013044
Calb2-IRES-Cre	The Jackson Laboratory	010774
Pdyn-IRES-Cre	The Jackson Laboratory	027958
Sst-IRES-Flp	The Jackson Laboratory	028579
TrpM5$^{-/-}$	Zhang et al., 2003	N/A
Otop1$^{-/-}$	Zhang et al., 2019	N/A
Oligonucleotides		
Sst *in situ* Probe	Advanced Cell diagnostics	404631-C2
Software and Algorithms		
Arduino	Arduino	https://www.arduino.cc
ImageJ (Fiji)	NIH	https://imagej.net/Fiji
MATLAB	MathWorks	https://www.mathworks.com

RESOURCE AVAILABILITY

Lead Contact

Further information and requests for resources and reagents should be directed to and will be fulfilled by the Lead Contact, Charles Zuker (cz2195@columbia.edu).

Materials Availability

This study did not generate new unique reagents.

Data and Code Availability

The data and custom code that support the findings from this study are available from the Lead Contact upon request.

EXPERIMENTAL MODEL AND SUBJECT DETAILS

Animals

All procedures were performed in accordance with the U.S. National Institutes of Health (NIH) guidelines for the care and use of laboratory animals, and were approved by the Columbia University Institutional Animal Care and Use Committee. Mice both male and female and at least 7 weeks of age were used in the study. The mouse strains used were purchased from the Jackson Laboratory: C56BL/6J (Stock Number 000664); *Sst-IRES-Cre* (Taniguchi et al., 2011) (013044); *Sst-IRES-Flp* (He et al., 2016) (028579); *Calb2-IRES-Cre* (Taniguchi et al., 2011) (010774); *Pdyn-IRES-Cre* (Krashes et al., 2014) (027958); The following strains used were generated in the Zuker lab: *TrpM5*$^{-/-}$ (Zhang et al., 2003); *Otop1*$^{-/-}$ (Zhang et al., 2019).

METHOD DETAILS

Viral constructs

The following AAVs were purchased from UPenn Vector Core and Addgene: AAV1-Syn-GCaMP6s-WPRE-SV40; AAV1-Syn-Flex-GCaMP6s-WPRE-SV40; AAV1-EF1a-DIO-hChR2(H134R)-eYFP-WPRE-hGH; AAV9-CaMKIIa-hChR2(H134R)-EYFP; AAV1-Syn-hChR2(H134R)-EYFP; AAV1-CMV-PI.EGFP-WPRE-bGH; AAV1-CAG-tdTomato; AAV1-CAG-Flex-tdTomato; AAV1-CAG-Flex-EGFP; AAV1-hSyn-eNpHR3.0-EYFP; The following AAVs were purchased from UNC Vector Core: AAV1-mCherry-Flex-dtA; AAV-Flex-TVA-mCherry. The following viruses were obtained from Janelia Vector Core: AAV1-fDIO-tdTomato; AAV1-hSyn-Cre; AAV1-CAG-Flex-GtACR1-P2A-EGFP; AAV-Flex-G(N2C)-mKate; RABV-N2C(ΔG)-GFP-EnvA.

Stereotaxic surgery

All the stereotaxic surgery procedures were carried out using aseptic technique. Mice were anesthetized with a mixture of ketamine and xylazine (100/10 mg kg^{-1}, intraperitoneally). Mice were then placed onto a custom-built stereotaxic frame with a closed-loop heating system to maintain body temperature. The skin was incised at the midline to expose the skull and a small craniotomy (< 1 mm) was made at the site above regions of interest. The viral constructs were loaded into a pulled glass capillary and injected using nanoliter system at 30 nL min^{-1} with the total volume of 30 nL (AAV-fDIO-tdTomato, AAV-Flex-tdTomato, AAV-Flex-EGFP, AAV-CAG-tdTomato,

AAV-CMV-EGFP), 200 nL (AAV-Syn-GCaMP6s and AAV-Syn-Flex-GCaMP6s), 50 nL (AAV-DIO-ChR2, AAV-CaMKIIa-hChR2 and AAV-Syn-ChR2) and 400 nL (AAV-Flex-dtA, AAV-hSyn-eNpHR3.0 and 1:1 mixture of AAV-Syn-Cre plus AAV-Flex-GtACR1). Viral injection is unilateral for photometry and optogenetic stimulation experiments and bilateral for ablation and photoinhibition experiments. The coordinates are: rNST (bregma −6.45 mm; lateral 1.1 mm; ventral 3.9 mm); bitter cortical field (bregma −0.35 mm; lateral 4.2 mm; ventral 2.7 mm); central amygdala (bregma −1.2 mm; lateral 2.9 mm; ventral 4.1 mm). For optogenetic implants, custom implantable fiber was made by gluing a 200 μm fiber bundle (NA = 0.39, Thorlabs) to a ceramic or metal ferrule (Thorlabs) and implanted unilaterally for activation of *Sst* and *Calb2* neurons or bilaterally for inhibition of projections from CeA above rNST (bregma −6.45 mm; lateral 1.1 mm; ventral 3.55 mm), and unilaterally above CeA (bregma −1.2mm; lateral 2.9mm; ventral 3.7mm) for activation of bitter cortical projections. For photometry implants, a custom-made fiber from Doric Lenses (200 μm or 400 μm O.D., NA = 0.48) was used and implanted ~100 μm above the GCaMP virus injection site. For pharmacological inhibition experiments, guide cannulas (26 gauge, PlasticsOne) were bilaterally implanted above central amygdala (bregma −1.2 mm; lateral 2.9 mm; ventral 3.7 mm). The ventral coordinates listed above are relative to the pial surface. All the implants were secured onto the skull using dental cement. A head-post was placed for all head-attached behavioral tests. After surgery, the animals were returned to home-cage and allowed to recover for at least 10 days before any test.

Intraoral fistula implantation

The procedures to implant intraoral fistula were adapted from a previously described procedure on rats (Phillips and Norgren, 1970). Basically, mice were anesthetized with ketamine and xylazine (100/10 mg kg^{-1}, intraperitoneally) and given antibiotic mixture (ampicillin and gentamicin) subcutaneously. An incision was then made on the side to expose the cranium. A curved needle was inserted under the skin along the lateral surface of the skull, and guided a catheter tubing subcutaneously to exit in the mouth lateral to the 4th molar. The mouth-end of catheter tubing was trimmed and the loose top end was secured onto the skull surface with dental cement. A head-post was placed for head-attached infusion. In the 2-3 days following implantation, mice were given antibiotic mixture daily to prevent infection.

Head-attached licking preference assay

Head-attached licking preference assay was performed essentially as described (Peng et al., 2015). Briefly, prior to test, thirsty animals (water deprived for 24-48 h) were acclimated to head-restraint and drinking from a motorized swing spout (2 training sessions per day for at least 2 days). Each trial started with a light flash, followed 1 s later by the spout swinging into position and a tone cue to indicate the onset of water delivery; after 5 s (during which mice could lick) the spout moved out of position. Training session at the acclimation phase lasted for 15 mins and consisted of 60 water trials (5-10 μL water per trial). To measure attractive responses (Figures 4D and 4E), before test, mice were mildly water deprived (24 h) and if necessary, supplied with water until exhibited, on average, 5-15 licks in 5 s licking window. During test, mice were provided with 2-5 μL of water at the beginning of each trial. To measure aversive response (Figures 4B and 4C), mice were water deprived for 36 h and provided with 5-10 μL of water per trial. Test session consisted of 10 water alone trials interspersed with 10 water plus laser trials (laser delivered upon licking). To examine the effect of photoinhibiting CeA-to-rNST projections (Figures 7E–7G), mice were water deprived for 36 h and tested in sessions consisting of randomly presented tastant (AceK, Qui, and AceK-Qui mix) trials; half of them were coupled with laser stimulation (laser on throughout the trial). Licking events were video tracked and determined by a custom-written MATLAB code. The control of the behavioral apparatus was performed with a program written in MATLAB interfacing with Arduino.

Freely moving licking preference assay

We measured taste preference in freely moving mice using a custom-built gustometer (Zhang et al., 2003). The behavior apparatus had a motorized shutter controlling mice's access to a drinking spout which consisted of a main tube enclosing 5 separate lines, each delivering a different tastant. Mice were water-deprived for 24-48 h and trained to drink from the spout in a 15 min session of free access to water (shutter open during the entire session and water delivered upon licking). To test attraction to sweet (Figure 3), mice were singly housed with 0.5-1 g of food and 1.5-2.5 mL of water 24 h before test, such that they were sufficiently hungry and slightly thirsty to prefer sweet over water. To test aversion to bitter and sour (Figure 3), mice were water deprived for 36 h before test such that they were sufficiently thirsty to be motivated to sample aversive tastants. To test salt preference (Figure 3), animals were injected with furosemide (50 mg kg^{-1}, intraperitoneally) 24 h prior to the test and provided with a salt-deficient diet (ENVIGO) (Chandrashekar et al., 2010); water was removed 6 h prior to the test. For measuring licking responses shown in Figure 1A, mice were singly housed with 0.5-1 g of food and 1.5-2.5 mL of water 24 h before testing. Test sessions consisted of 60 trials with randomly presented tastants. The licking events were collected by a capacitive touch sensor and analyzed by a custom-written MATLAB code. The behavioral apparatus was controlled by a custom-written MATLAB software interfacing with Arduino. Dose-response behavioral assay (Figure S1A) was performed using a Davis MS160-mouse gustometer (Glendinning et al., 2002) with 6 independent channels. Animals were semi-restrained in a small chamber within the gustometer. Animals were water deprived 24-48 h, habituated for 2-3 days and then tested over the following 3-4 days. Animals were tested with 2 test sessions, consisting of 48 trials each, with 28 randomly presented sucrose alone trials and 4 trials of each type (Qui concentration) of sucrose-quinine mix (high sucrose alone to mix ratio was necessary to motivate animals to lick). Lick counts, inter-lick interval and lick latency were automatically recorded for each trial.

Two-bottle preference assay

Two-bottle preference assay was performed essentially as described previously (Nelson et al., 2001). Briefly, in the first day of 24 h period, the baseline preference for two bottles both containing water was determined. AceK then replaced water in the less preferred bottle for subsequent measurement. The consumption of AceK (1.5 mM and 20 mM) solutions versus water over 24 h was measured. The preference ratio was calculated as V_{AceK}/V_{water} where V_{AceK} was volume drunk from the AceK bottle and V_{water} was volume drunk from the water bottle.

Three-port and four-port taste discrimination task

Three-port taste discrimination assay: mice were trained in a customized three-spout chamber within a sound-attenuating cubicle (Med Associates) to report the identity of tastant cues at the middle spout, for each trial in 100-trial sessions, by choosing between the right or the left spout for water reward. Mice were water deprived 24-48 h to begin training. Thereafter, they generally received water only during ~2 sessions/day of training. Each trial began with the middle-spout shutter opening, allowing access to the tastant cue. Mice were given 60 s to initiate sampling. Upon initiation, right/left shutter opened, and the mouse had 4 s to receive water reward. For the first 2-3 days of training, only the shutter to the correct side opened upon cue-sampling initiation, guiding the mouse to the correct spout (right for sweet and left for bitter or vice versa). Thereafter, both shutters opened simultaneously, forcing the mouse to choose right or left. Correct choices resulted in water reward, after which the shutters closed; the next trial began after 10 s. Incorrect choices resulted in the shutters immediately closing and a punishment of 5 s "timeout" (in addition to the 10 s inter-trial interval). Tastant cues were psuedo-random. Initial training was with sweet (4 mM AceK) and bitter (1 mM quinine). After mice reached ~90% accuracy (~1 week), a third cue, 3 mM NaCl, was added to their training (followed by water reward at the sweet side for *Sst* experiments and at the bitter side for *Calb2* experiments). After training *Sst* mice with 3 mM NaCl (additional 1-2 weeks), in order to prepare them for the test session and hinder learning during the test session that there is no reward on laser trials mice were trained for an additional 1-2 days with sessions in which they received water reward on only 70% of the trials. The other 30% of the trials were treated as test trials for which regardless of which side they chose, the shutters immediately closed and there was no time-out punishment. *Calb2* mice were given the 70%-reward training before being exposed to 3 mM NaCl, and close to testing they were given brief training with 3 mM NaCl as necessary for them go to the bitter side in response to 3 mM NaCl. Test sessions consisted of 86 pseudo-randomized trials, with 10 trials of 3 mM NaCl (all rewarded if correct) and 10 trials of 3 mM NaCl + laser (all unrewarded, regardless of choice). The other 66 trials were divided between sweet and bitter trials, 70% rewarded trials and 30% unrewarded trials.

Four-port taste discrimination assay: mice were trained in three stages using a customized behavioral chamber consisting of a tastant sampling port at its front side and three water reward ports (port 1, 2 and 3) on the opposite side (see Figure 4I). Mice were first trained to identify sweet (4 mM AceK) versus salt (60 mM NaCl) by choosing between port 1 or 2. A correct choice was rewarded with 5 s of water and the incorrect one resulted in 5 s of "timeout" (see above for three-port assay). This training was carried out for ~2 sessions a day with 120 trials per session for ~2 weeks. After the accuracy of reporting sweet and salty stimuli exceeded 80%, mice were switched to salty-bitter training sessions in which they learned to report salt (60 mM NaCl) and bitter (1 mM quinine) by going to port 2 or 3 for the water reward. This training lasted about 4-5 weeks. Intermittently, mice were retrained in sweet-salty sessions to prevent extinction. After the accuracy of reporting salty and bitter reached more than 80%, mice were subjected to the sweet-salty-bitter training sessions until they reliably reported each of the three stimuli (additional 4-5 weeks). Test sessions consisted of 10 unrewarded trials of 3mM NaCl, 10 unrewarded trials of 3mM NaCl + laser, and rewarded sweet, salty and bitter trials (27 trials each).

For both assays, licks were registered via a capacitive touch sensor (MPR121), and fluid delivery, laser, and shutters were controlled via an Arduino board by a custom MATLAB program which also controlled data acquisition.

DTA mediated cell ablation

For data shown in Figures 3B–3G, mice were first measured for their preference for sweet, bitter, sour and salty stimuli in the freely moving licking preference assay. After initial taste preference was measured, mice were bilaterally injected with 400 nL AAV-mCherry-Flex-dtA in the rNST to ablate selective neuronal population. Mice were recovered for 4-6 weeks, allowing sufficient DTA expression and cell ablation before testing for their post-DTA taste preference. In Figure 3H, controls consisted of *Calb2-cre* negative mice receiving the same dose of DTA virus injection.

Photostimulation

For all ChR2 stimulation experiments, 473 nm light pulses (diode-pumped solid-state laser, Shanghai Laser & Optics Century Co.) were delivered via a custom-made optic cable (Thorlabs) and controlled by a custom-written MATLAB code via Arduino. Laser intensity was kept at 1-20 mW at the tip of fiber. In photoactivation behavior experiments, one lick triggered 1 s (50 pulses) of light stimulation (20 Hz, 20 ms per pulse) and licks during light stimulation extended the stimulation until 1 s after the final lick. For infusion coupled with light-stimulation of the bitter cortical field and bitter cortical projection in CeA, light was delivered in a 10 s time window when tastant was infused. For photoinhibition experiments, 589 nm (eNpHR) or 473 nm (GtACR1) light (diode-pumped solid-state laser, Shanghai Laser & Optics Century Co.) was split using branching fiber-optic patch cord (Doric lenses) for bilateral illumination. Constant light (3-10 mW at the tip of fiber) was maintained throughout the light-on trials.

Infusion and lick fiber photometry

For photometry recording during intraoral infusion in awake animals (Figures 2, 5, 7A, S2A, S2D–S2F, and S5), at least 3 days after intraoral fistula implantation, mice were adapted to head restraint and intraoral infusion by receiving water through intraoral fistula (0.8 mL min^{-1}, 15 mins) using a syringe pump. After 3 consecutive daily adaption sessions, mice were subjected to experimental session consisting of multiple tastant infusion trials while being fiber photometry recorded. An infusion trial consisted of 10 s of infusion of tastant by syringe pump at the speed of 0.8 mL min^{-1}, preceded by 30 s pre-infusion interval and followed by 30 s post-infusion interval. During pre and post infusion intervals, water was flowing at the speed of 0.8 mL min^{-1}. For photometry during licking (Figures S2B and S2C), the animals were head-restrained and trained to lick from a motorized swing spout (see method of head-attached licking preference assay). Prior to recording sessions, animals were water deprived for 36 h to motivate licking. To record taste evoked response in *Sst* and *Calb2* neurons in rNST during licking, the animals were given 0.5 s to lick from tastants and a dry spout in a recording session; this short lick time window (0.5 s) enforced similar lick counts across stimuli.

Bulk Ca^{+} dependent GCaMP fluorescence signals were measured using fiber photometry as described previously (Gunaydin et al., 2014). Briefly, 465 nm and 405 nm light from connectorized light-emitting diodes (Doric Lenses) was combined in a connectorized fluorescence mini-cube and delivered into the brain. The emission fluorescence was then focused onto a femtowatt photodetector (NewPort) before outputting to an amplifier. The amplified signals were digitized by LabJack U6-Pro and recorded using custom MATLAB code via LabJack U6-Pro with 100 Hz sampling rate. The collected data were analyzed by custom MATLAB code. They were first extracted and subject to a low-pass filter at 2 Hz. A least-squares linear fit was then applied to produce a fitted 405 nm signal. The dF/F was calculated as: (F-F0)/F0, where F0 was the median fitted 405 nm signal in 3 s time window before the onset of tastant infusion. The calcium transients were identified using validated statistical measures (the median and Qn estimator) (Rousseeuw and Croux, 1993) and the area under the curve (AUC) was calculated by integrating fluorescence signal under identified calcium transients. The traces displayed were after fluorescence data were smoothed using a moving average method and downsampled to 5 Hz.

Pharmacological Inhibition

For pharmacological silencing in photometry recording, 400 nL of a cocktail of AMPA receptor antagonist NBQX (2,3-dioxo-6-nitro-1,2,3,4-tetrahydrobenzo[f]quinoxaline-7-sulfonamide, 25 mM in 0.9% NaCl, Tocris Bioscience) and NMDA receptor antagonist AP5 (D-(-)-2-Amino-5-phosphonopentanoic acid, 38 mM in 0.9% NaCl, Tocris Bioscience) was bilaterally infused into the CeA using a 1 μL Hamilton through an internal cannula (PlasticsOne) inserted into the guide cannula above the amygdala. 20 mins after infusion, mice were recorded for the photometry response to tastants delivered through intra-oral cannula. For pharmacological silencing in freely moving licking assay, mice were bilaterally infused with 200-300 nL of NBQX (12.5 mM), rested for 20-90 mins, and tested for their licking responses. Prior to behavioral testing for taste preference, the animals were water deprived for 36 h to motivate licking. As a control, the same animals were infused with equivalent volume of isotonic saline (0.9% NaCl) and recorded/tested with identical experimental procedures.

Whole brain clearing

The whole brain was cleared by cubic method essentially as described previously (Susaki et al., 2014, 2015; Wang et al., 2018). In brief, mice were perfused with phospho-buffered saline (PBS) containing 10 U/ml heparin and 4% paraformaldehyde (PFA). Brains were then post-fixed in 4% paraformaldehyde for 3 h. The fixed brains were first washed with PBS 3 times before immersion in cubic reagent 1 (diluted 1:2 in water) overnight. The brains were then switched to and incubated in reagent 1 for 7-10 days with new reagent 1 changed every other day. The reagent 1-treated brains were washed with PBS and degassed in PBS overnight before being transferred into cubic reagent 2 (diluted 1:2 in PBS). For the final clearing, the brains were immersed in reagent 2 containing TO-PRO3 (1:5, 000, Thermo Fisher Scientific) for 3-7 days. Prior to imaging, the brains were equilibrated with a mineral and silicone oil mix (1:1). Images were acquired with a light-sheet fluorescence microscope (UltraMicroscope) with a 1.3X objective. The images were registered to a reference atlas using ANTs and further processed in ImageJ.

Brain slice electrophysiological recordings

Sst-cre mice were infected with AAV-CAG-Flex-tdTomato in the rNST and AAV-CamKII-ChR2-EYFP in the GCbt. *Calb2-cre* mice were infected with AAV-CAG-Flex-tdTomato in the rNST and AAV-CamKII-ChR2-EYFP in the GCbt or AAV-Syn-ChR2-EYFP in the CeA. After viral infection, mice were allowed 2-4 months for recovery (2-4 months for *Sst-cre* mice and 2-3 months for *Calb2-cre* mice), enabling sufficient expression of ChR2 in the axonal terminals in the rNST. Mice were anesthetized with ketamine/xylazine (100/10 mg kg^{-1}, intraperitoneally), and then transcardially perfused with ice-cold oxygenated slicing solution. Coronal slices containing the rNST were sectioned into 300 μm thickness using a vibratome (VT-1000S, Leica) in ice-cold sucrose-based slicing solution (in mM: 213 sucrose, 26 $NaHCO_3$, 10 dextrose, 2.5 KCl, 2.0 $MgSO_4$, 2.0 $CaCl_2$, and 1.23 NaH_2PO_4, aerated with 95% O_2 / 5% CO_2). Slices were transferred to oxygenated artificial cerebrospinal fluid (ACSF; composition in mM: 126 NaCl, 26 $NaHCO_3$, 2.5 KCl, 2.0 $MgSO_4$, 2.0 $CaCl_2$, 1.25 NaH_2PO_4 and 25 dextrose, 315 mOsm, adjusted to pH 7.4) and incubated at 32°C for 40 minutes, then maintained at room temperature until use. Neurons were visualized using an upright infrared differential interference contrast microscope (BX51WI, Olympus). *Calb2* or *Sst* neurons in the rNST infected with AAV-CAG-Flex-tdTomato were identified by fluorescence. Whole-cell voltage clamp recordings were performed at 32°C with an Axopatch 200B amplifier and a Digidata 1440A (Molecular

Devices). The patch electrode (2.8 - 3.5 MΩ) was filled with intracellular solution (in mM: 125 CsCl, 5 NaCl, 10 HEPES, 0.6 EGTA, 10 QX-314 Chloride, 4 Mg-ATP, 0.3 Na-GTP, 290 mOsm, adjusted to pH 7.2). Data were sampled at 10 kHz, filtered at 2 kHz, and analyzed with Clampex10.4 software (Molecular Devices). Pulses of photostimulation (1 ms, 470 nm) were controlled by Clamplex software and delivered through an X-Cite XLED1 (Lumen Dynamics).

To record postsynaptic currents evoked by light pulses, the membrane potential of *Calb2* or *Sst* neurons in rNST was held at −70 mV in voltage clamp mode (Figure 6). GABAergic inhibitory postsynaptic currents were blocked by PTX (Picrotoxin, 50 μM) applied through bath. Glutamatergic excitatory postsynaptic currents were blocked by bath application of DNQX (6,7-dinitroquinoxaline-2,3-dione, 10 μM). To distinguish EPSCs and IPSCs directly, in another set of experiments (Figure S6), we used the following intracellular solution (in mM: 115 CsMeSO4, 4 NaCl, 10 HEPES, 0.3 Na-GTP, 4 MgATP, 0.3 EGTA, 10 QX-314, 0.2% Biocytin, 290 mOsm, adjusted to pH 7.2). With this intracellular solution, EPSCs and IPSCs were recorded at voltage clamp mode by holding the neurons at −70mV and −10mV, respectively. Monosynaptic connection was defined by the postsynaptic currents with onset latencies less than 15 ms. Onset latency was defined as the time from light stimulus to the time at 10% of the peak amplitude of a postsynaptic event. To confirm monosynaptic connections, we applied TTX (Tetrodotoxin, 1 μM) and 4-AP (4-Aminopyridine, 1 mM) in the bath and the latencies and peak amplitudes of the evoked postsynaptic currents remained unchanged.

Monosynaptic retrograde tracing

100 nL of AAV-Flex-TVA-mCherry and AAV-Flex-G(N2C)-mKate mixture (1:1) was injected into the rNST of *Sst-cre* or *Calb2-cre* animals. 2– 3 weeks later, rNST of these animals were infected with 100 nL RABV-N2C(ΔG)-GFP-EnvA. The animals were sacrificed in 7 – 14 days to identify and examine presynaptic neurons across the brain by histology.

Histology

Viral expression and placement of optic implants were verified at the termination of the experiments using DAPI counterstaining of 100 μm coronal sections (Prolong Gold Antifade Mountant with DAPI, Invitrogen). For fluorescent *in situ* hybridization, fresh frozen brains were sectioned at 16 μm thickness and processed for mRNA detection using RNAscope (Advanced Cell Diagnostics) according to the manufacturer's instructions. Immunostaining was performed as described before. Briefly, mice were intracardially perfused with PBS followed by 4% PFA. Brains were dissected, fixed in 4% PFA overnight at 4°C, and then sliced coronally at 50 or 100 μm thickness. The brain sections were permeabilized and blocked with 10% normal donkey serum (EMD millipore) in PBS with 0.3% Triton X-100, incubated with anti-*Calb2* primary antibody (Immunostar 24445, 1: 500) at 4°C overnight, and labeled with fluorescent tagged secondary antibody at room temperature for 2 hr. To label biocytin filled neurons after slice recording, brain slices were fixed with 4% PFA for 30 mins at 4°C, blocked with 10% normal donkey serum and stained with Alexa Fluor 647 conjugated streptavidin (Invitrogen S32357, 1:500) for 2 hr at room temperature. Images were acquired using an Olympus FluoView1000 confocal microscope. Cell numbers were counted manually.

QUANTIFICATION AND STATISTICAL ANALYSIS

Statistical tests were performed using ANOVA followed by Tukey post hoc analysis, unpaired t test or paired t test when appropriate. Each statistical test used was indicated in the respective figure legends. $p < 0.05$ was considered to be statistically significant.

Supplemental Figures

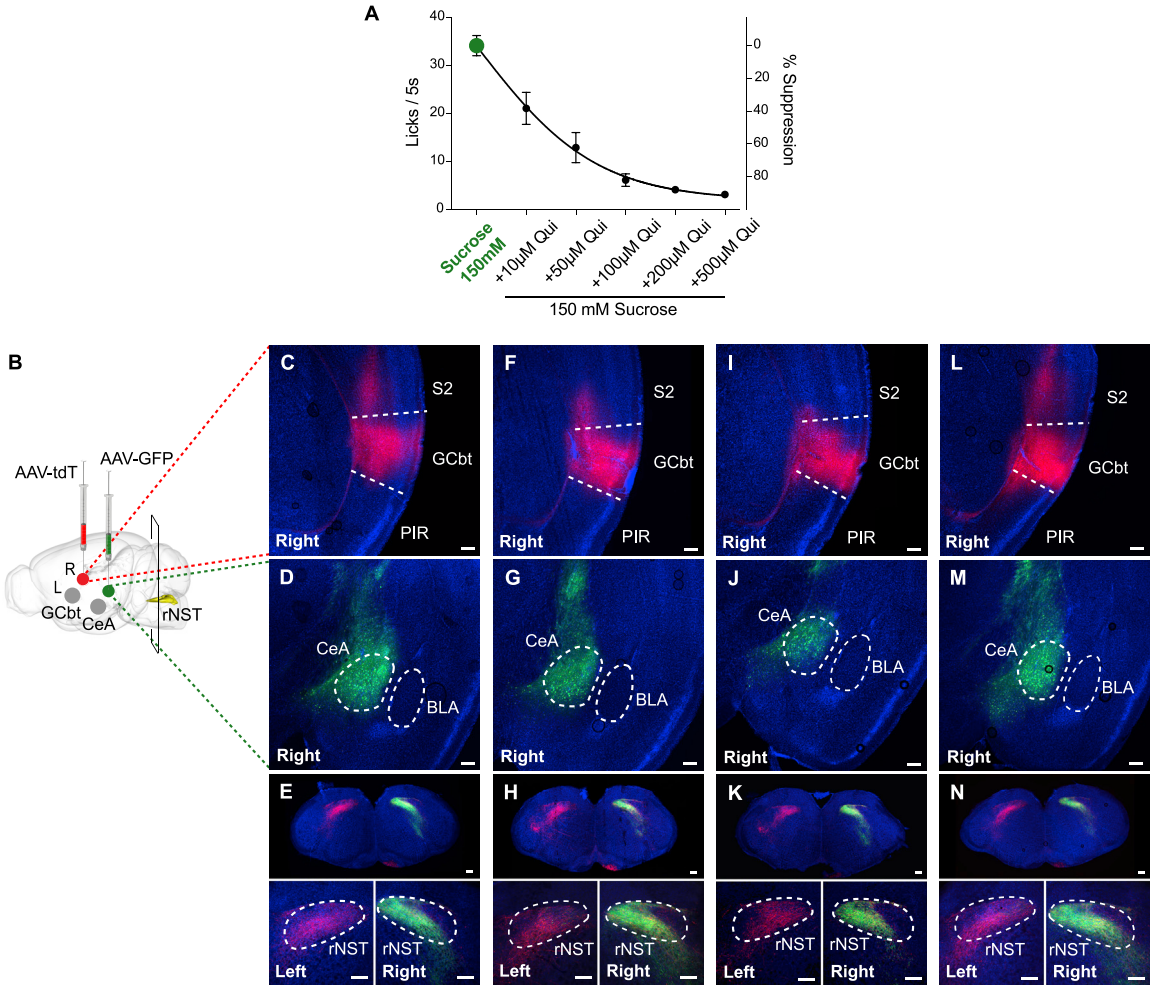

Figure S1. Bitter Suppression of Sweet Attraction and Projections from Bitter cortical field and CeA to the rNST, Related to Figure 1

(A) The dose response illustrates the impact of increasing concentrations of a bitter tastant (Qui) in suppressing the attraction to 150 mM sucrose; this concentration of sucrose was chosen as it triggers ~50% of maximal licking responses in a sucrose dose-response assay (Zhao et al., 2003). See STAR Methods for details. Shown are taste preference results for 150 mM sucrose (green), and 150 mM sucrose plus 10 μM, 50 μM, 100 μM, 200 μM and 500 μM Qui; n = 6 mice, values are means ± SEM. The mean lick data were fitted with a sigmoidal function. The right axis indicates % suppression, relative to the licking responses to 150 mM sucrose alone.

(B) To trace projections from GCbt and CeA to rNTS, anterograde tracers were injected into GCbt and CeA (AAV-tdTomato and AAV-GFP, respectively) and their projections were analyzed by serial coronal sectioning and confocal imaging; n = 4 mice. R and L refer to right and left hemispheres. S2: secondary somatosensory cortex; Piri: Piriform cortex; BLA: basolateral amygdala.

(C-E) Shown are tracing results from one of the four animals. (C) AAV-tdTomato injection site in GCbt (bregma −0.3 mm). (D) AAV-GFP injection site in CeA (bregma −1.2mm). (E) Projection targets in rNST (dashed outline, bregma −6.5mm). Shown are sections at increasing magnification highlighting target areas from GCbt (red) and CeA (green). GCbt projects predominantly to contralateral rNST (i.e., R side was injected and terminals project to L rNST), In contrast, CeA projects primarily to ipsilateral rNST. GCbt also sends projections to other brain areas including entorhinal cortex, parabrachial nucleus, and nucleus accumbens (data not shown); CeA also sends projections to parabrachial nucleus, bed nucleus of the stria terminalis and lateral hypothalamus (data not shown). Scale bars, 200 μm.

(F-N) Equivalent results from 3 additional animals.

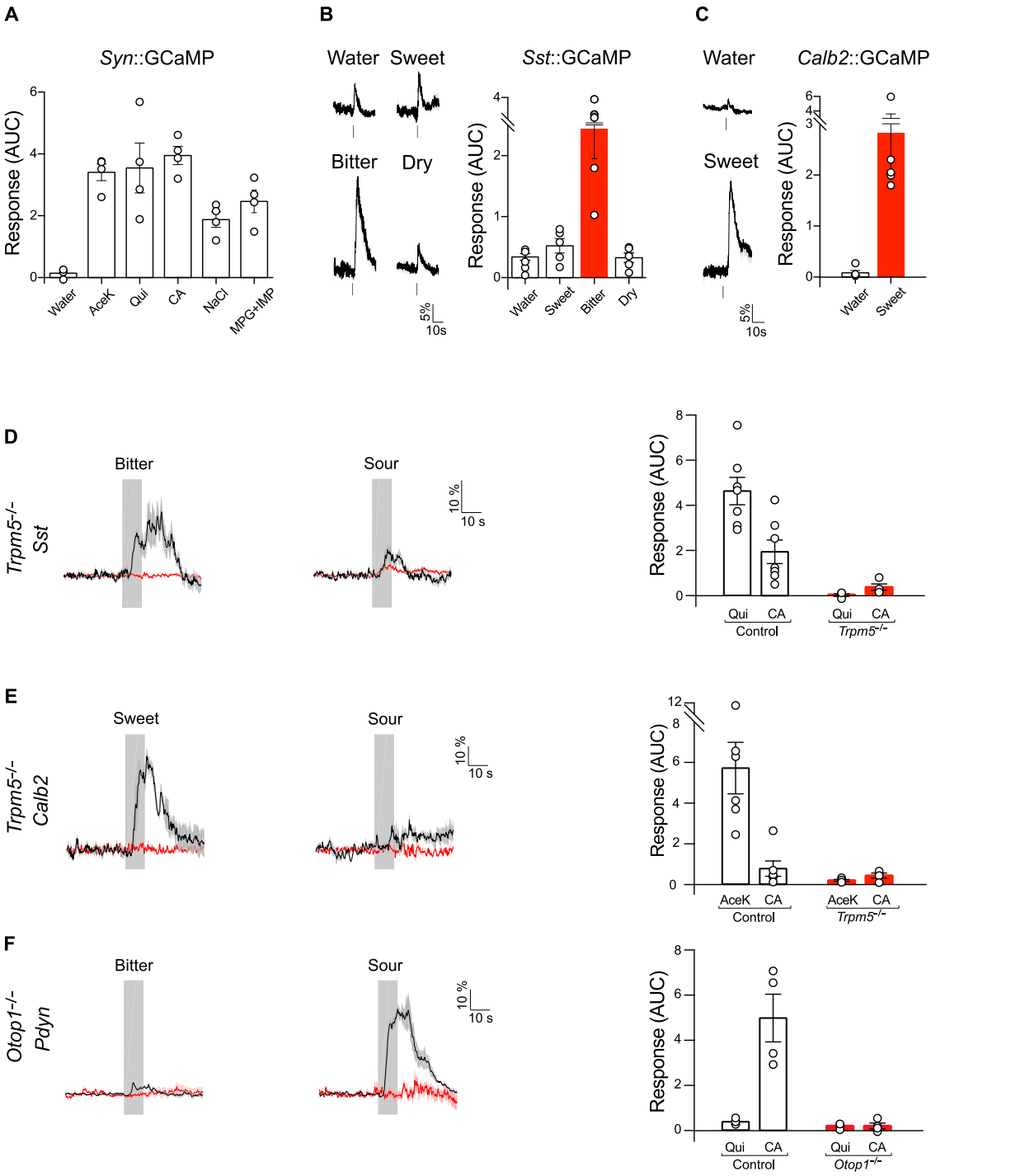

Figure S2. Responses of rNST Neurons in Wild-Type and Taste Mutants, Related to Figure 2

(A) Shown is the quantification of taste responses in animals expressing a GCaMP reporter (AAV-syn-GCaMP6) in rNST neurons. Tastants: Sweet, 20 mM AceK; Bitter, 5 mM Qui; Sour, 50 mM CA; Salty, 60 mM NaCl; Umami, 50 mM MPG + 1 mM IMP. n = 4 animals.

(B) Small responses from *Sst* neurons to water and sweet are also seen in dry-licking trials. Animals were water deprived for 36 h prior to the recording session to motivate licking. Shown are fiber photometry recordings from *Sst* neurons in the rNST in response to 0.5 s presentations of 10 mM AceK, 100 μM cyx, water, and a dry spout. AUC: area under the curve; n = 5 animals. Values are means ± SEM.

(C) *Calb2* neurons are not significantly activated by licking. Animals were water deprived for 36 h prior to the recording session to motivate licking. Shown are fiber photometry recordings from *Calb2* neurons in the rNST in response to 0.5 s presentations of water or 20 mM AceK. AUC: area under the curve; n = 5 animals.

(legend continued on next page)

Values are means ± SEM. We also note that *Calb2* neurons are not significantly activated by umami (Figure 2D), another attractive stimulus that triggers strong appetitive responses (Zhao et al., 2003).

(D) Shown are responses of *Sst* neurons to bitter (5 mM Qui) and Sour (50 mM CA) tastants in wild-type controls (black traces) and *Trpm5* knockout animals (red traces). Note that the response to bitter was largely abolished in *Trpm5* knockouts. The small activity seen in response to acid stimulation arises from acid-evoked activation of bitter GPCRs (Barretto et al., 2015), and expectedly, is greatly diminished in the absence of bitter TRC signaling (compare responses to acid in the control versus *Trpm5* mutants). In contrast, responses from sour TRCs are unaffected by *Trpm5* mutations (Zhang et al., 2003 and see panel F below). Control: n = 7; *Trpm5* knockout: n = 4. Values are means ± SEM. Unpaired t tests: Qui (Control versus *Trpm5*) $p < 0.001$; CA (Control versus *Trpm5*) $p < 0.05$. The control data presented comes from Figure 2C.

(E) Responses of *Calb2* neurons in wild-type control and *Trpm5* knockout animals. Note that the responses to sweet stimuli (20 mM AceK) were abolished in the *Trpm5* knockouts. Control: n = 6; *Trpm5* knockout: n = 4. Values are means ± SEM. Unpaired t tests: AceK (Control versus *Trpm5*) $p < 0.01$; CA (Control versus *Trpm5*) $p > 0.4$. The control data presented comes from Figure 2D.

(F) Sour and bitter responses of *Pdyn*-expressing neurons in the rNST (see also Zhang et al., 2019). *Pdyn* neurons are selectively tuned to sour taste, and the responses are ablated in animals lacking the sour taste receptors OTOP1 (Teng et al., 2019; Zhang et al., 2019). Tastants, 50 mM CA and 5 mM Qui. Wild-type controls, n = 4, *Otop1* knockouts, n = 4. Values are means ± SEM. Unpaired t tests: CA (Control versus *Otop1*) $p = 0.02$; Qui (Control versus *Otop1*) ($p > 0.05$).

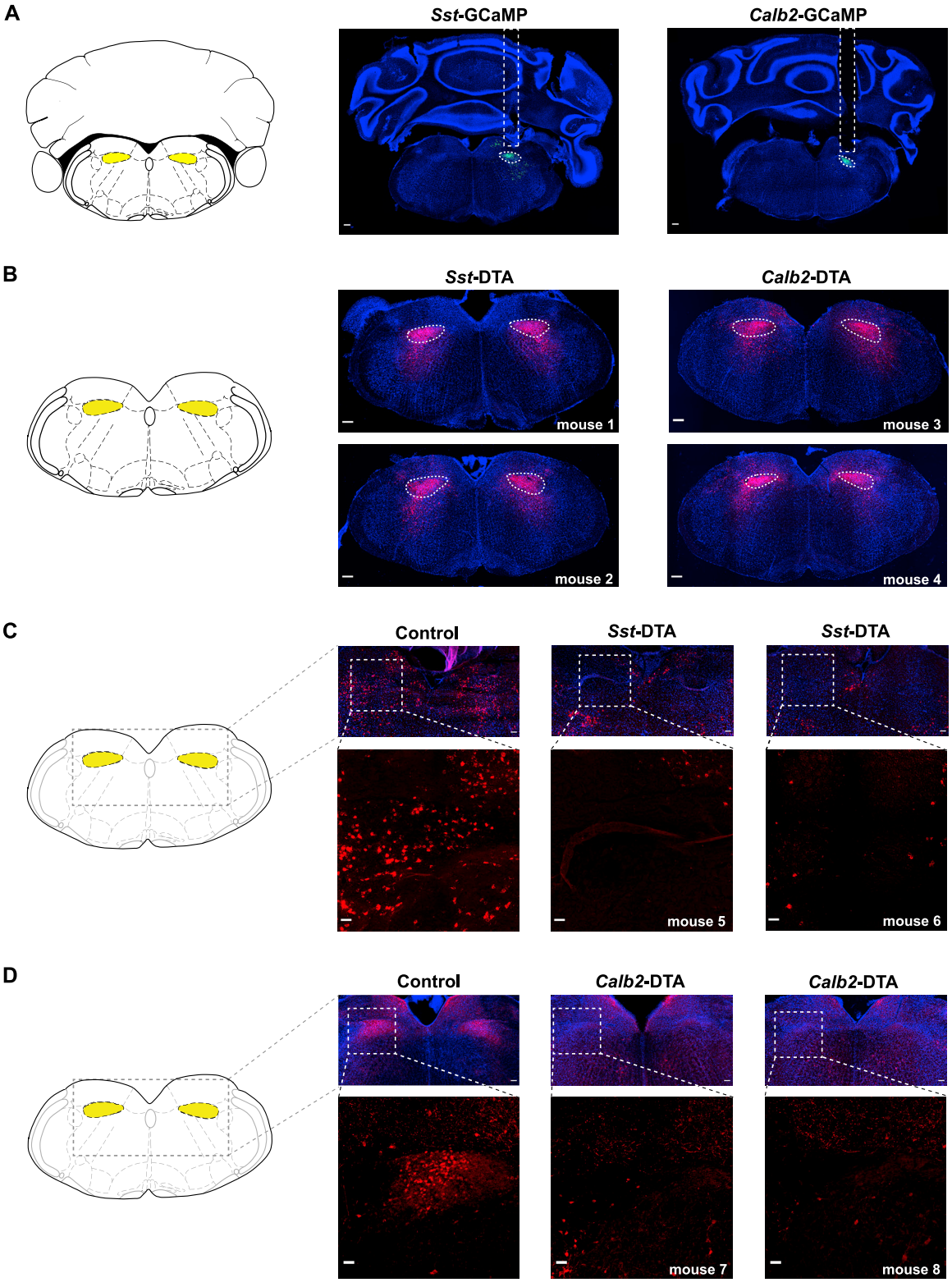

Figure S3. Histological studies, Related to Figures 2 and 3

(A) Diagram of a coronal section highlighting rNST (in yellow, left panel). The right panels show the location of the recording fibers in two independent animals expressing GCaMP in the rNST (one in *Sst* neurons and the other in *Calb2* neurons); note the position of the fiber (dashed lines) immediately above the rNST. Scale bars, 200 μm.

(legend continued on next page)

(B) Diagram of a coronal section highlighting rNST (in yellow, left panel). The right panels show mCherry reporter expression in the rNST of animals bilaterally infected with AAV-Flex-DTA. Note the selective expression in rNST (dashed outline). Scale bars, 200 μm.
(C) *In situ* hybridization with *Sst* probes demonstrates the selective loss of *Sst* neurons in rNST after DTA induced cell death. Left panel, diagram of a coronal section highlighting the rNST (in yellow). Right panels show increasing magnifications of the *in situ* signals for *Sst* transcript (pseudocolored as red) in the rNST of one wild-type control and two sample *Sst-cre* animals infected with AAV-Flex-DTA. As expected, *Sst* neurons are ablated and the corresponding *Sst* signals is lost. Scale bars: upper panels, 100 μm; lower panels: 50 μm.
(D) Immunofluorescence staining demonstrates selective loss of *Calb2* neurons in the rNST of *Calb2-cre* animals after bilaterally targeted DTA infection (AAV-Flex-DTA). Left panel, diagram of a coronal section highlighting rNST (in yellow). Right panels show increasing magnifications of *Calb2* neurons marked by an anti-Calb2 antibody (pseudocolored as red) in the rNST of one wild-type control and two *Calb2-cre* animals infected with AAV-Flex-DTA virus. Note that the loss of *Calb2* immunofluorescent signals. Scale bars: upper panels, 100 μm; lower panels: 50 μm.

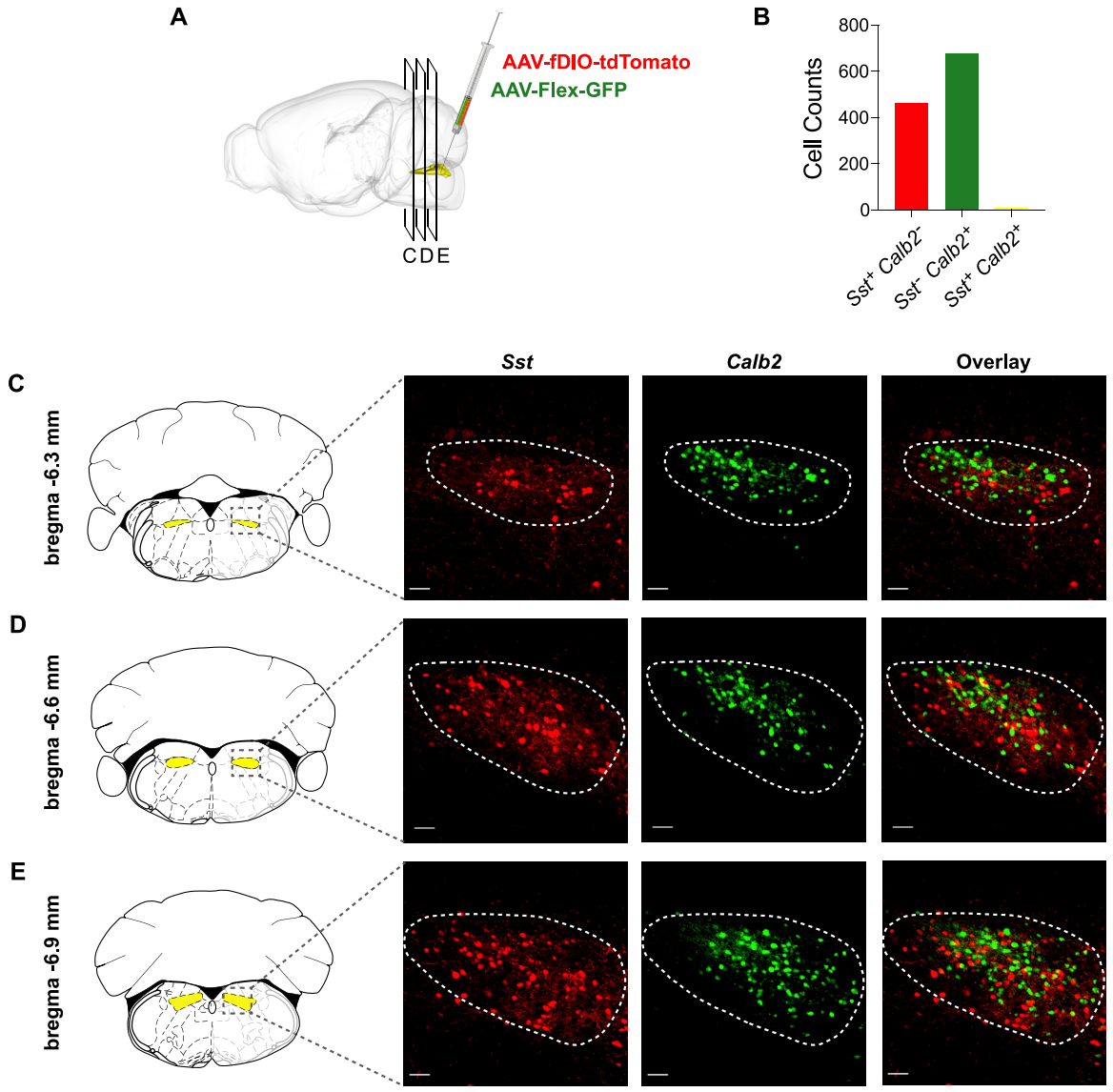

Figure S4. *Sst* and *Calb2* Are Expressed in Separate Populations of rNST Neurons, Related to Figures 2 and 3

(A) Schematic of double labeling strategy. The rNST of *Sst-flp*; *Calb2-cre* animals (i.e., a "double reporter" mouse line) were infected with a Flp-dependent tdTomato reporter (AAV-fDIO-tdTomato) and a Cre-dependent GFP reporter (AAV-Flex-GFP).

(B) Quantification of neurons expressing *Sst* (tdTomato), expressing *Calb2* (GFP) and expressing both. A total of 1146 neurons (from 4 different animals) were analyzed and examined for reporter expression. In each animal, three representative sections spanning the anteroposterior extent of rNST were selected for analysis (panels C-E). Only 7 of the 1146 neurons (< 1%) were labeled with both reporters; 463 were labeled with tdTomato (expressing *Sst*) and 676 with GFP (expressing *Calb2*).

(C-E) Shown are *Sst*-expressing neurons (marked by tdTomato, red) and *Calb2* neurons (marked by GFP, green) in the rNST (dashed outline) at three different coronal planes (C: bregma −6.3mm, D: bregma: −6.6mm, E: bregma: −6.9mm). The right panel shows the overlap (i.e., neurons expressing both genes). Scale bars, 50 μm.

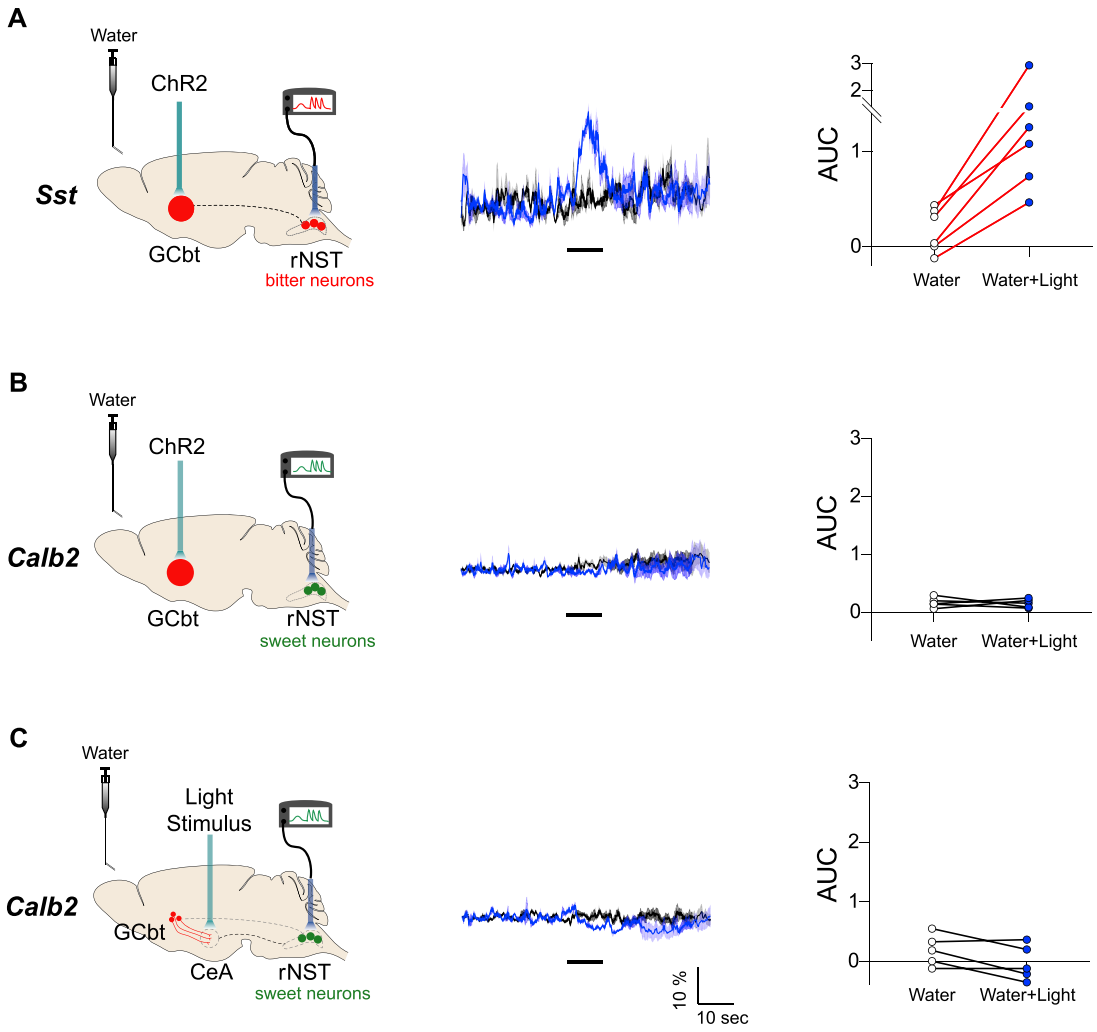

Figure S5. Responses of *Sst* and *Calb2* Neurons to Activation of GCbt and GCbt-to-CeA Projections, Related to Figure 5

These control experiments examined the responses of *Sst* and *Calb2* neurons following activation of GCbt and GCbt-to-CeA projections in the absence of sweet or bitter stimuli (compared to Figure 5).

(A) GCbt was transduced with an AAV-CamKII-ChR2 virus, and a stimulating fiber (ChR2) was placed over the GCbt (red). The same animals expressed GCaMP6s in bitter *Sst* neurons in the rNST. Middle panel shows a sample recording illustrating responses evoked by ChR2 stimulation of GCbt in the absence of tastants (water was flowed via an intraoral cannula). As expected, activation of GCbt stimulates *Sst* neurons (via the positive feedback); blue = response in the presence of GCbt stimulation; black = response in the absence of GCbt stimulation (water but no light). Traces are average (solid color) ± SEM (shade). Scale: ΔF/F. The right panel shows the quantitation of responses; n = 6 animals. Paired t test: $p = 0.01$.

(B) Activation of GCbt has no significant effect on the response of *Calb2* neurons in the absence of a sweet stimulus. Shown is a sample recording; blue = response in the presence of GCbt stimulation; black = response in the absence of GCbt stimulation (water but no light). Traces are average (solid color) ± SEM (shade). Scale: ΔF/F. The right panel shows the quantitation of responses; n = 5 animals. Paired t test: $p > 0.8$.

(C) Activation of bitter cortical projections in CeA has no significant effect on the response of *Calb2* neurons in the absence of a sweet stimulus. Shown is a sample recording; blue = response while stimulating GCbt projections to CeA; black = response in the absence of stimulation of GCbt projections to CeA (water but no light). Traces are average (solid color) ± SEM (shade). The right panel shows the quantitation of responses; n = 5 animals. Paired t test: $p > 0.08$.

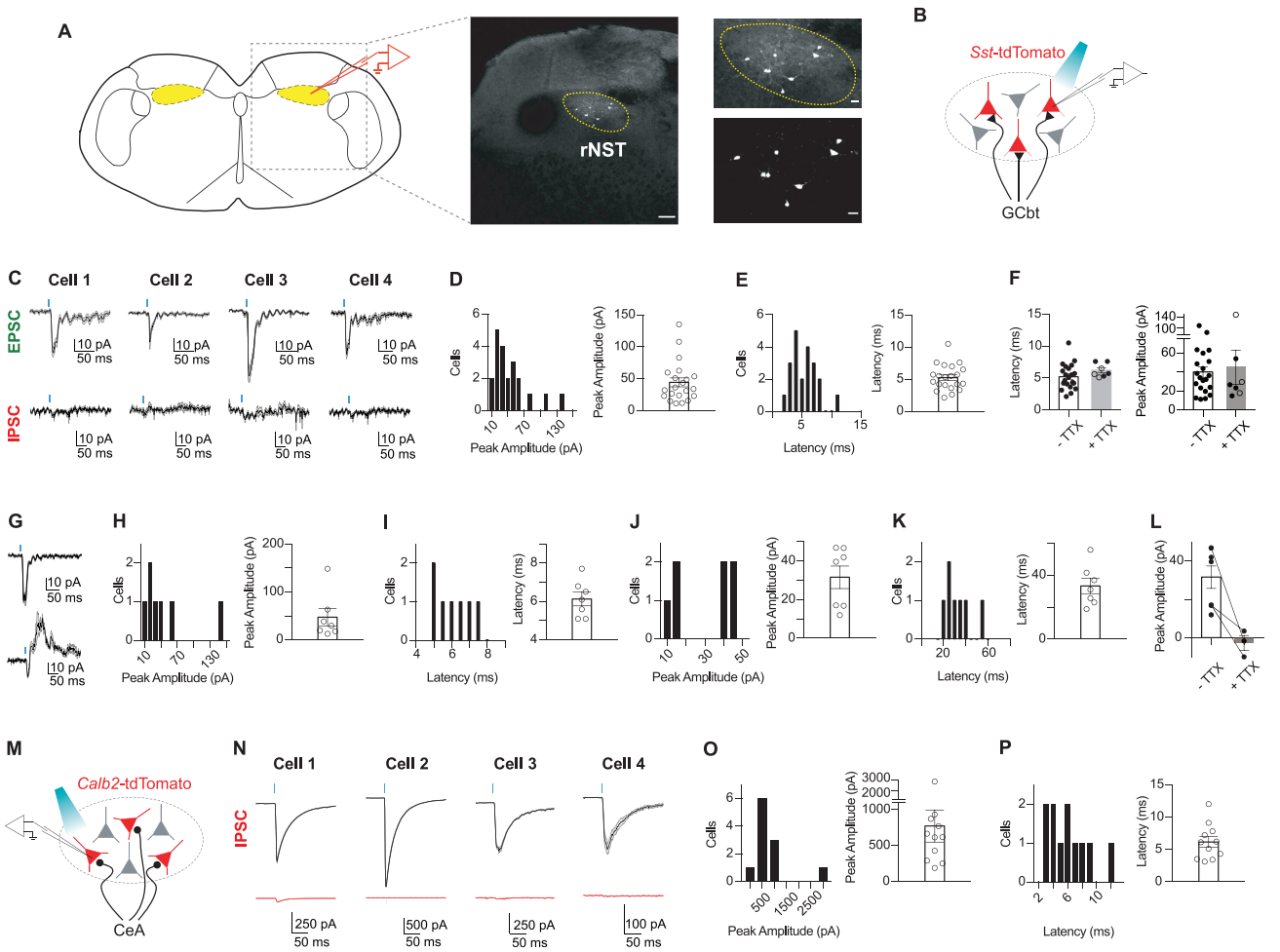

Figure S6. Physiological Recording in rNST Slices, Related to Figure 6

(A) Diagram of the brainstem slice preparation showing the location of sample patched neurons in the rNST. The patched cells were filled with biocytin and stained with streptavidin Alexa 647 (pseudocolored as white).

(B) Schematic of whole cell patch-clamp recording of *Sst*-expressing neurons in the rNST while optogenetically activating GCbt projections to the rNST.

(C) Sample recordings of four *Sst* neurons in the rNST that receive feed-forward excitation from GCbt. Shown are EPSCs (upper panels) and IPSCs (lower panels) in response to optogenetic stimulation of the GCbt projections (the traces show average ± SEM). Membrane potentials were held at −70 mV or −10 mV to record EPSC or IPSC, respectively. The blue bars denote the onset and duration of the light stimulus. (D) Histogram and bee-swarm plot of peak amplitudes; n = 21 neurons. (E) Quantification of latency of EPSC responses. The latency was defined as the time between the onset of the optogenetic stimulation and the 10% rise point of the EPSC. (F) Summary graph of EPSC latency and peak amplitude in the absence (n = 21) and presence (n = 7) of TTX. Note that the EPSC latency and peak amplitude remain unchanged in the presence of TTX either without (open circles) or with 4-AP (solid circles), as would be expected for monosynaptic inputs. Unpaired t test: p = 0.2 (latency); p = 0.7 (peak amplitude).

(G) Sample recordings of a *Sst* neuron in the rNST that received feed-forward excitation and inhibition from GCbt (of a total of 28 neurons, 21 showed only excitatory responses, and 7 had both excitatory and inhibitory; see text for details). Shown are EPSC (upper panel) and IPSC (lower panel) in response to optogenetic stimulation of GCbt projection in rNST (the traces show average ± SEM). (H) Histogram and bee-swarm plot of EPSC peak amplitudes; n = 7 neurons. (I) Quantification of EPSC latencies. (J) Histogram and bee-swarm plot of IPSC peak amplitudes of the same 7 neurons. (K) Quantification of IPSC latencies. (L) TTX treatment abolishes IPSC currents. Shown is the summary graph of IPSC peak amplitudes before and after TTX treatment; 3 neurons were tested.

(M) Schematic of whole cell patch-clamp recording of *Calb2*-expressing neurons in the rNST while optogenetically activating CeA terminals.

(N) Sample recordings of four *Calb2* neurons in the rNST (upper traces). All 4 neurons were inhibited after activation of CeA inputs, and the IPSC responses were blocked by treatment with PTX (red traces below IPSCs). (O) Histogram and bee-swarm plot of IPSC peak amplitudes, n = 11 neurons. (P) Quantification of IPSC latencies.

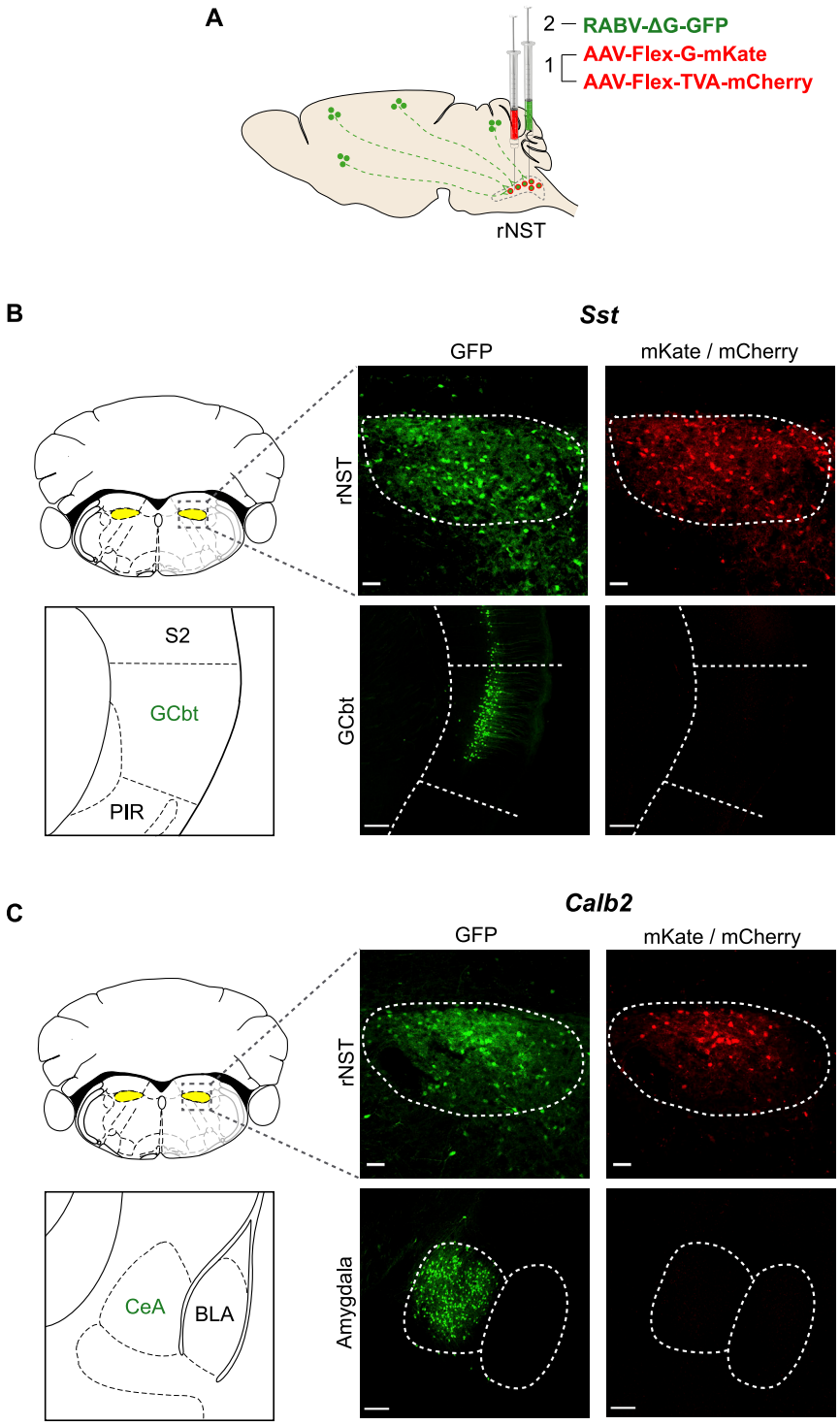

Figure S7. Retrograde Tracing from *Sst* and *Calb2* Neurons, Related to Figure 6

(A) Schematic of retrograde monosynaptic tracing. The rNST of *Sst-cre* and *Calb2-cre* animals were infected with the monosynaptic tracing reporters AAV-Flex-G-mKate and AAV-Flex-TVA-mCherry, followed by RABV-ΔG-GFP (see text and STAR Methods for details).

(B) *Sst* neurons in the rNST receive monosynaptic input from neurons in GCbt. Upper panels, enlarged views of the rNST (dashed outline) in the *Sst-cre* animals infected with AAV-Flex-G, AAV-Flex-TVA and RABV-ΔG-GFP. Scale bars, 50 μm. Lower panels show neurons receiving the retrograde *trans*-synaptic viral reporter (RABV-ΔG-GFP) in GCbt. Note the absence of mCherry/mKate^{+} neurons in GCbt and selective retrograde labeling of cortical layer 5 (GFP^{+}) of GCbt as the source of inputs to *Sst* neurons in the rNST.

(legend continued on next page)

Sample quantification (bregma −0.3 mm): GFP$^+$ neurons in GCbt = 124 ± 13.4; mCherry/mKate$^+$ neurons in GCbt: 0.8 ± 0.3 (mean ± SEM). n = 4 animals. Scale bars, 100 μm.

(C) *Calb2* neurons in the rNST receive monosynaptic input from neurons in CeA. Upper panels, enlarged views of rNST in the *Calb2-cre* animals infected with AAV-Flex-G, AAV-Flex-TVA and RABV-ΔG-GFP. Scale bars, 50 μm. Lower panels show neurons receiving the *trans*-synaptic viral reporter (RABV-ΔG-GFP) in CeA. Note the absence of mCherry/mKate$^+$ neurons in the amygdala, and the selective retrograde labeling of CeA (GFP$^+$) as the source of input to *Calb2* neurons in the rNST. Sample quantification (bregma −1.2 mm): GFP$^+$ neurons in CeA: 269.3 ± 23.0; mCherry/mKate$^+$ neurons in CeA: < 1 (0.5 ± 0.3). n = 4 animals. Scale bars, 100 μm.